

KRISTJAN LEBEN

Long-term diagenetic transformation and
carbon sequestration potential of Ca-rich
oil shale ash waste deposit sediments



KRISTJAN LEBEN

Long-term diagenetic transformation and
carbon sequestration potential of Ca-rich
oil shale ash waste deposit sediments



UNIVERSITY OF TARTU
Press

Department of Geology, Institute of Ecology and Earth Sciences, Faculty of Science and Technology, University of Tartu, Estonia.

This dissertation is accepted for the commencement of the degree of Doctor of Philosophy in Geology at the University of Tartu on the 8th of February 2021 by the Scientific Council of the Institute of Ecology and Earth Sciences, University of Tartu.

Supervisor: Riho Mõtlep, Department of Geology, University of Tartu, Estonia

Opponent: Ron Zevenhoven, Professor in Engineering Thermodynamics and Modelling, Åbo Akademi University

This thesis will be defended at the University of Tartu, Estonia, Chemicum, Ravila 14A, room 1019, on the 9th of April 2021 at 12:15.

Publication of this thesis is granted by the Institute of Ecology and Earth Sciences, University of Tartu and by the Doctoral School of Earth Sciences and Ecology created under the auspices of the European Social Fund.



European Union
European Social Fund



Investing
in your future

ISSN 1406-2658

ISBN 978-9949-03-566-3 (print)

ISBN 978-9949-03-567-0 (pdf)

Copyright: Kristjan Leben, 2021

University of Tartu Press

www.tyk.ee

CONTENTS

LIST OF ORIGINAL PUBLICATIONS	6
1. INTRODUCTION.....	7
2. MATERIALS AND METHODS	11
2.1. Oil shale ash	11
2.2. Ash sediment materials.....	13
2.3. Analytical methods.....	14
3. RESULTS AND DISCUSSION	16
3.1. Composition and long-term diagenesis of hydrated oil shale ash sediments at waste deposits	16
3.1.1. Chemical and phase composition	16
3.1.2. Ash sediment diagenesis.....	22
3.2. Carbonation of Ca-rich ash waste.....	27
3.2.1. Carbonate carbon and oxygen stable isotope composition of ash waste	27
3.2.2. Mineral carbonation potential of Ca-rich ash waste.....	33
4. CONCLUSIONS.....	40
REFERENCES.....	42
SUMMARY IN ESTONIAN	52
ACKNOWLEDGEMENTS	57
PUBLICATIONS	59
CURRICULUM VITAE	113
ELULOOKIRJELDUS.....	114

LIST OF ORIGINAL PUBLICATIONS

This thesis is based on the following published papers. These papers are referred to in the text by their respective Roman numerals.

- I Leben, K.; Mötlep, R.; Paaver, P.; Konist A.; Pihu, T.; Paiste, P.; Heinmaa, I.; Nurk, G.; Anthony, E.; Kirsimäe, K. (2019). Long-term mineral transformation of Ca-rich oil shale ash waste. *Science of the Total Environment* 658, 1404–1415. <https://doi.org/10.1016/j.scitotenv.2018.12.326>.
- II Leben, K.; Mötlep, R.; Paaver, P.; Konist A.; Pihu, T.; Kirsimäe, K. (2020). Geochemical study of stable carbon and oxygen isotopes in landfilled Ca-rich oil shale ash. *Estonian Journal of Earth Sciences* 69 (3), 134–142. <https://doi.org/10.3176/earth.2020.09>.
- III Leben, K.; Mötlep, R.; Konist A.; Pihu, T.; Kirsimäe, K. (2021). Carbon dioxide sequestration in power plant Ca-rich ash waste deposits. *Oil Shale* 38 (1), 65–88. <https://doi.org/10.3176/oil.2021.1.04>.

The author's contribution:

Paper I: The author was primarily responsible for planning the original research and data collection. He participated in conducting mineralogical-geochemical analysis as well as the interpretation of analytical results, the synthesis of analytical data and the writing of the manuscript.

Paper II: The author was primarily responsible for planning the research, running experiments, data collection, also contributing to the writing of the manuscript.

Paper III: The author was primarily responsible for planning the original research, also participating in data collection and the interpretation of analytical results, the synthesis of mineralogical-geochemical-structural data. He coordinated the writing of the manuscript.

1. INTRODUCTION

Energy industries using solid fossil fuels, such as coal, lignite, peat and oil shale, are responsible for producing a large share of the global greenhouse gas (GHG) emissions as well as large quantities of solid mining and combustion residues. These residues are often chemically reactive and frequently deposited in open ponds or waste deposits. The potential environmental impact of such dumped wastes depends on their composition, which is the combination of the geological origin of fuel, combustion/retorting processes, methods of residue disposal and overall climatic conditions (Fulekar and Dave, 2007). However, these residues can and should be beneficially reused, for example in the manufacture of concrete and construction materials as well as by harnessing their potential in carbon capture and storage (CCS) (Bobicki et al., 2012; Lieberman et al., 2018; McCarthy and Dhir, 1999). The beneficial utilization rates vary from country to country, ranging from only a few percent to almost complete utilization.

In the light of current European CO₂-trade policies, and more importantly, long-term planning to achieve future climate goals (e.g., Nationally Determined Contribution to the Paris Agreement Update to the NDC, 2020), the usage of fossil fuels will inevitably diminish in the coming decades. However, a carbon neutral economy can be realized by 2050 (European Commission, 2019) only if we consider and apply all means capable of effectively reducing the CO₂ budget, including the implementation and optimization of various CO₂ sequestration techniques.

Different options that could help mitigate climate change, including carbon capture and storage (CCS), are already being considered worldwide (Aminu et al., 2017; Bui et al., 2018; IPCC, 2007, 2005; Sanna et al., 2014; Yamasaki, 2003; Zhang et al., 2020). Firstly, carbon dioxide can be deposited underground in suitable rock formations, dissolved in saline aquifers, or adsorbed onto the organic matter in coal or shale formations. However, it requires the geological formation to have specific properties to ensure the stability of storage and minimize the possibility of CO₂ leakage back into the atmosphere. Underground deposition of CO₂ is widely used in the process of Enhanced Oil Recovery (EOR), but the additional oil obtained during the process is likely to nullify any extra mitigation by such means.

Another CCS method involves binding carbon dioxide in geologically stable carbonate minerals, i.e. mineral carbonation, which occurs naturally during the slow weathering of silicate minerals and their reaction with atmospheric CO₂. This process can be employed on waste materials that contain natural alkaline earth metal oxide-bearing minerals (mainly CaO and MgO), such as various ultramafic mine wastes (Kelemen et al., 2020; Oskierski et al., 2013; Pronost et al., 2011; Wilson et al., 2014), or industrial process waste, e.g. coal or oil shale ash (OSA), steel slag and other waste products (Bobicki et al., 2012; Ochedi et al., 2020; Olajire, 2013; Pan et al., 2012; Sanna et al., 2014; Yörück et al., 2020). Sequestration can be carried out by carbonation, either *in-situ* at suitable

geological sites and waste deposits or *ex-situ* at designated plants or CO₂ point sources before the final deposition of the material (Yadav and Mehra, 2021). Various types of industrial wastes with a high content of chemically active alkaline metal oxides, such as CaO and MgO, can provide an effective and readily available opportunity for CO₂ sequestration. These waste streams usually originate from big industrial CO₂ emitters and the proximity to the source favours the possible exploitation of waste streams for CO₂ sequestration. Although the volume of such waste is comparatively small and can only mitigate part of the emitted carbon dioxide, it could constitute an additional and easily accessible reactive resource for CO₂ sequestration. For example, it has been shown that coal fly ash has a high CO₂ binding potential with reported sequestration capacity values ranging from 7.66 kg/ton to 230 kg/ton (Dindi et al., 2019; Montes-Hernandez et al., 2009).

Oil shales (OS), a type of kerogenous fossil fuel, represent a particular case. OS deposits are found worldwide, but they are exploited only in a few countries, mostly due to their low energetic value and environmental concerns. Even OS with the best possible quality, such as the Estonian kukersite type oil shale with an energetic value of 8–12 MJ/kg (Ots, 2006), leaves ca. 45–53% of solid residues upon combustion (Konist et al., 2016; Loo et al., 2018; Maaten et al., 2017b, 2017a). This is much more than the 5–20% of solid waste left in typical coal firing. The Estonian energy sector has relied on the oil shale industry for a long time, leading to two opposite consequences. On one hand the use of oil shale has secured Estonia's energy independence ever since the 1960s. On the other hand, the industry is also by far the largest national producer of solid waste and emitter of greenhouse gases, responsible for over 70% of all CO₂ emitted in Estonia (Statistics Estonia, 2016). EU statistics has placed Estonia as no 1 emitter of CO₂ among member states, with 18.6 metric tonnes per capita (Crippa et al., 2019). In 2019, however, Estonia's power production and, consequently, the CO₂ emissions from oil shale industry nearly halved (Eesti Energia, 2019). This was a direct consequence of an increase in carbon dioxide emission allowance prices under the European Union Emission Trading Scheme (EU ETS), which makes fossil fuels less competitive on the open Nord Pool energy market where Estonia is trading (Elering, 2014). Nevertheless, Estonia's oil shale operations are currently the largest in the world.

In Estonia, about 15 million tonnes of calcareous OS has been mined annually in the recent years, which has led to the generation of 6–8 million tonnes of Ca-rich ash. Only a few percent of the ash is reused, mainly in cement production and in agriculture as a liming agent. The rest is landfilled near the power plants (Konist et al., 2016; Mõtlep et al., 2010). The transportation of ash to disposal sites in water slurry initiates ash hydration and results in a variety of secondary Ca-minerals – Ca-hydroxide (portlandite), ettringite, hydrocalumite, etc. Those secondary phases, along with the clinker minerals formed in ash during combustion, provide sufficient self-cementation of the ash material for building high self-sustaining steep-walled waste depositories reaching up to 50 meters. However, the long-term behaviour and stability of these waste deposits is determined

by the sequential diagenetic recrystallization of initial secondary phases. This process needs to be assessed to avoid waste heap structural failures and the potential leaching of hazardous components, as well as to evaluate the carbon sequestration potential of the ash material via direct or indirect carbonation of several secondary phases.

Oil shale ash produced by the combustion of calcareous oil shale may contain up to 27 wt% of free lime (CaO_{free}) (Pihu et al., 2019), constituting a potential CO_2 sink. Although the mineral matter in OS feed contains an average of 50–70 wt% of carbonate minerals, not all of its non-volatile decomposition products remain as CaO in ash, but react further to form Ca- and Ca/Mg-silicates, Ca-sulphate and other non-carbonate minerals. MgO, which forms after the decomposition of dolomite, is primarily found as periclase and Ca/Mg-silicates, such as merwinite and akermanite (Leben et al., 2019 – PAPER I; Uibu et al., 2009). Thus, not all of the CaO from the carbonate mineral decomposition is readily available for CO_2 capture, at least not in the short term. Several of these secondary Ca-phases in ash, as well as its hydration products, are metastable in open environment, becoming decomposed/recrystallized over time. Liira et al. (2009), Mõtlep et al. (2010) and Velts et al. (2013) have assessed the transformation and alkalinity potential of OS ash sediments and have suggested, based on modelling and mineralogical data, that the transformation of hydrated ash sediments in open conditions is governed by the carbonation of portlandite, a hydration product of CaO. However, due to the slow transport of CO_2 into ash waste deposits, the full neutralization of 45 m thick ash sediment deposits via carbonation would require hundreds of thousands of years (Mõtlep et al., 2010). That is in stark contrast with theoretical calculations and empirical ash carbonation experiments.

The theoretical CO_2 capture capacity of PC oil shale ash is 350–500 kg of CO_2 per tonne of ash, 30–50% of which is solely based on free lime (Uibu and Kuusik, 2014). However, previous laboratory carbonation experiments have estimated that only 37 kg of CO_2 per tonne of ash, equating to only about 4–5% of total CO_2 or about 20% of carbonate CO_2 emitted during oil shale combustion, is bound back by the carbonation of oil shale ash sediments (Kuusik et al., 2001). A much higher potential of up to 11% of total emissions or 209 kg of CO_2 per one tonne of ash (including neutralizing transport water) has been achieved in subsequent laboratory-scale experiments (Uibu et al., 2009). In contrast to laboratory-scale experiments that often reach an equilibrium state, the carbonation reactions in natural conditions within ash deposits are not completed due to the burial of ash sediment under continuous deposition of new material, environmental constraints and inhibited transport (availability) of CO_2 through solidified ash layers (Leben et al., 2019 – PAPER I; Mõtlep et al., 2010). In field conditions, it has been suggested that ca. 5–6% of CO_2 emitted during oil shale combustion is bound back from the atmosphere in ash waste deposits and sediment ponds (Konist et al., 2016).

Transformation of hydrated Ca-rich OS ash and its initial self-cementation is well characterized at laboratory scale (Liira et al., 2009; Raado et al., 2014; Uibu et al., 2016). However, its long-term stability under natural conditions and the

extent of carbonation reactions taking place within the ash deposits themselves have remained poorly constrained. Several *in-situ* studies of the mechanical and mineralogical stability of waste deposits (Nguyen et al., 2015; Yvon et al., 2006) have focused on short-term changes, which occur after only a few years. In open conditions, however, mineral and chemical transformations can occur for extended periods of time, until waste reaches equilibrium with the environment. Furthermore, the diagenetic processes, potentially influencing the phase composition of the ash sediment, can negatively impact the previously estimated CO₂ sequestration ability of the deposited material by producing mineral phases stable enough in such ambient conditions or initiating non-CO₂ related diagenesis.

This thesis aims to characterize the composition and CO₂ binding potential of the oil shale ash waste sediments of power plant ash deposits that have been accumulated over a period of nearly 50 years and subjected to transformations in a highly alkaline open environment. In most cases, the stability and long-term behaviour of such deposits is studied by means of short-term laboratory experiments, which fall short of describing and predicting long-term changes taking place in these materials.

The main objectives of the dissertation are:

- to characterize the long-term diagenetic transformation of Ca-rich ash wastes under highly alkaline conditions and assess the long-term stability of ash deposits of this type;
- to determine the main sources of carbon in natural mineral carbonation reactions in oil shale ash deposits;
- to assess the long-term CO₂ binding capacity in Ca-rich oil shale ash deposits at the oil shale firing power plants' over nearly 50 years of sedimentation, as well as the mineral-chemical transformation and the estimation of the remaining sequestration potential for accelerated *in-situ* carbonation.

The hypothesis of this work suggests that the fast deposition of Ca-rich oil shale ash under subsequent ash layers hinders its contact with atmospheric carbon dioxide and maintains the long-lasting highly alkaline conditions inside the ash deposits. These environmental conditions lead to natural alkaline activation and the formation of polymeric semicrystalline phases, which can increase the mechanical stability and structural integrity of the deposits, but at the same time reduce the CO₂ sequestration potential of this material.

2. MATERIALS AND METHODS

2.1. Oil shale ash

The fossil fuel used in Estonian power plants and shale oil retorts is a Ordovician kukersite oil shale (OS), which is a kerogenous solid fuel with a high mineral content and a low calorific value of 8–12 MJ/kg (Ots, 2006). The kukersite OS mineral part is characterized by a high Ca content, because the OS seams occur in a normal marine carbonate succession (Bauert and Kattai, 1997).

In the recent years, Estonia's annual mining output has remained around 15 Mt of calcareous OS, while about 6–8 Mt of ash is produced annually by the OS energy industry (Eesti Energia, 2019; Konist et al., 2016; Mõtlep et al., 2010). High-temperature (>1200–1400 °C) pulverized combustion (PC) technology was the main method for processing OS up until 2018, but ever since 2004 PC has been gradually replaced by circulated fluidized bed combustion (CFBC) technology operating at 700–800 °C. The lower temperature combustion allows complete burn-off of organics, but only partial thermal dissociation of dolomite and calcite, i.e. carbonate minerals dominant in oil shale. Dolomite's decomposition into CaO, MgO and CO₂ begins at *ca.* 550 °C, whereas the decomposition of calcite, which produces most of the CaO and CO₂, starts at *ca.* 620 °C and reaches a maximal rate at 895–900 °C (L'vov, 2007). During the retorting of shale oil in a solid heat carrier (SHC) retorting process, the temperature is kept lower, in the range of 400–500 °C. The spent shale containing a considerable amount of residual organics is burnt at 700–800 °C for a short time, before it is reintroduced as a heat carrier into the retort (Kann et al., 2004; Sedman et al., 2012). PC boilers emit up to 1 tonne CO₂ per tonne of fuel (Gavrilova et al., 2005), but CFB combustion emits up to 13% less (Loo et al., 2018), largely due to the lower extent of carbonate decomposition in low-temperature combustion. The extent of decomposition is 0.97 in PC and 0.60 in CFBC (Arro et al., 2006). Carbonate decomposition during combustion and retorting processes produces ash rich in reactive free CaO and MgO (Bityukova et al., 2010; Kuusik et al., 2005; Mõtlep et al., 2010). The high reactivity of alkali oxide phases initiate hydration reactions already during the hydraulic transportation of ash to the depositories and continue with more complex transformation reactions in the ash deposits that proceed over decades (Leben et al., 2019 – PAPER I; Mõtlep et al., 2010; Pihu et al., 2019). The aging of the ash containing free CaO and MgO, also known as quick lime and periclase, is mainly governed by carbonation in open air conditions (Liira et al., 2009). These reactions proceed through the hydration of CaO to Ca(OH)₂ (portlandite) which further reacts with the (atmospheric) CO₂ to form a stable calcium carbonate (CaCO₃) phase. An important aspect of the carbonation is the neutralization of the ash material that, at the initial hydration step, has a pH of 12–13, which is controlled by portlandite equilibrium. Upon progression of carbonation, pH gradually decreases to ~8, reaching equilibrium with calcite.

The solid residues from the older SHC technology (e.g., Enefit140 and Petroter) still contain up to 2–3% of residual organics due to the incomplete burn-off of the solid residues (Talviste et al., 2013). By contrast, in the most modern shale oil retorting plant (Enefit280, commissioned in 2012), where the SHC retort is combined with a CFBC unit, final ash is virtually free of organic residues (Neshumayev et al., 2019; Paaver et al., 2017). The composition of Enefit140 SHC retorting ash formed at adjacent oil retorting plants is poorly known, because ash cannot be extracted from the retort units in a dry state. However, the technology used at these retorts is similar to that of Petroter SHC retorts and the composition of dark grey to black ash forming at Petroter is in principal similar to the fly ash produced in CFBC boilers at power plants. The most notable difference is the presence of the Ca-sulphide phase (CaS – oldhamite) in oil retorting ash, instead of Ca-sulphate (anhydrite) occurring in CFBC ash (Sedman et al., 2012; Talviste et al., 2013). However, CaS is unstable under atmospheric conditions and quickly becomes dissolved and subsequently oxidized into sulphate (Kann et al. 2004). Therefore, given the similar composition of the retorting and power plant ashes, notable compositional variation is not expected. That is further supported by a much lower share of retorting ash (about 20% of total) to combustion ash (Kuusik et al., 2012).

The ash forming at power plants and shale oil retorts is transported mixed with water (water/solid ratio ca. 20:1) to waste disposal ponds on waste depositories next to the processing plants, where the slurry solidifies (Pihu et al., 2012). As a result of nearly 70 years of operation, more than 300 million tonnes of ash has been deposited in up to 45 m high plateau-like waste depositories, covering more than 20 km² (Mõtlep et al., 2010).

The Eesti Power Plant (EPP) and the Balti Power Plant (BPP), located in Northeast Estonia, are the largest oil shale operations, commissioned along with adjacent ash depositories in 1969 and 1959, respectively (Fig. 1). The general composition of ash deposited in the sedimentary ponds at the depositories has remained the same over the whole period of power plant operation. SHC oil retorting ash has been co-deposited alongside oil shale PC ash since the 1980s. From 2004 onward ash from lower-temperature CFBC boilers has been co-deposited with PC ash. By now it has almost completely replaced PC ash. CFB ash therefore contribute to the sediments in the upper few metres of the studied sections. The ash depository at EPP also receives ash from the new Auvere PP, commissioned in 2016, as well as the newest Enefit-280 shale oil plant that has been in operation since 2012 (Golubev, 2003; Pihu et al., 2019). These ash deposits have been in continuous use ever since the commissioning of their respective PPs. The composition of fuel (calcareous oil shale) has not changed over time.

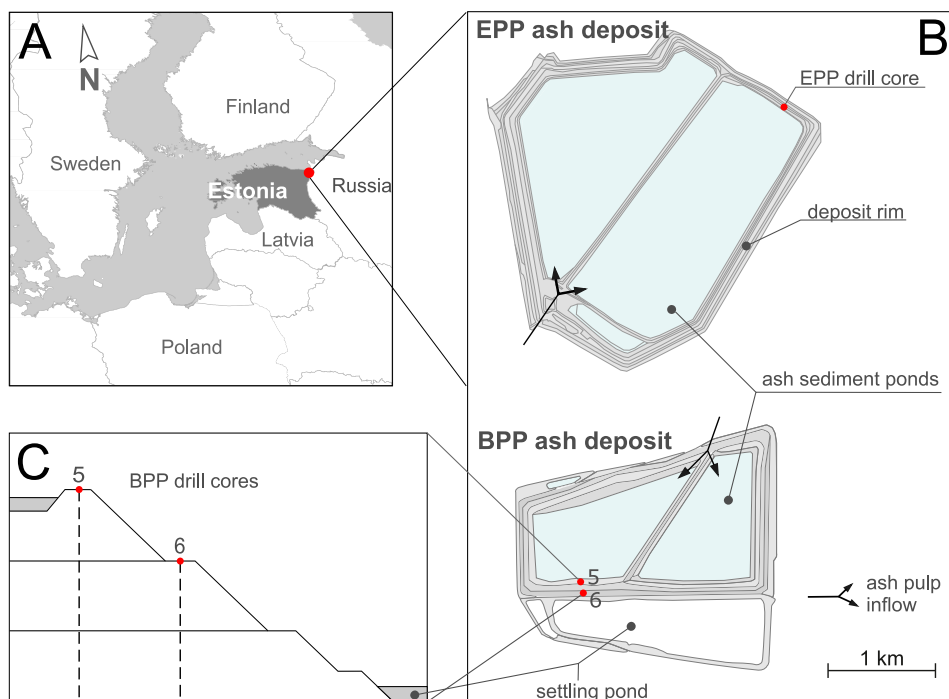


Figure 1. The location and overview of ash waste deposits and drill cores: A) the location of oil shale power plants and studied ash depositories; B) the studied drill core locations on the EPP and BPP ash depositories; C) the schematic cross-section of BPP rim and the location of drill cores No. 5 and 6.

2.2. Ash sediment materials

Studied material was obtained from three drill cores penetrating the ash deposits in northeast Estonia (Fig. 1): drill core No. 2 at Eesti Power Plant (EPP) and drill cores No. 5 and 6 at Balti Power Plant (BPP). The total thickness of the EPP deposit at the drilling site was 37.5 m, the core penetrating the whole deposit and reaching the underlying Quaternary peat and sand at the depth of 41.5 m. The groundwater level in the drill hole during the drilling operation was measured at a depth of 6.6 meters below surface. Altogether 69 samples for mineral and 34 for chemical composition were taken across the whole sequence of the EPP ash deposit. Drill cores No. 5 and 6 in the ash depository at BPP reached 32 m and 26 m in depth, respectively, while the groundwater level was measured at 16–18 m during drilling in drill hole No. 5 and at 6–8 m in drill hole No. 6. The mineral composition of BPP ash sediments was analyzed in the 42 samples obtained from drill core No. 5 and 28 samples from drill core No. 6, with a sampling interval of 0.5–1.5 meters over the ash sediment successions. The sampled material represents bulk ash sediment that was mixed during the dam building process.

Additionally, an experimental laboratory study of oil shale ash carbonation was undertaken to study the initial rapid changes in carbon and oxygen isotope composition of bulk ash sediment carbonate part. During the experiment the fresh fly ash from the electrostatic precipitators of the CFBC boiler at Balti Power Plant was fully hydrated and thereafter stored in open air conditions. Dried ash bulk samples were taken for isotope analysis after two weeks and three months of curing.

The precise share of the retorting ash in the ash samples taken from the EPP ash depository is unknown but its relative contribution (absent, low, medium, high) was estimated in studied samples by assessing sediment colour (see data table online at <https://doi.org/10.15152/GEO.491>; Leben et al., 2020 – PAPER II). The hydrated ash from power plants is white to pale beige-grey, whereas the ash from SHC retorts is dark-grey to black.

2.3. Analytical methods

The X-ray diffraction (XRD) analysis of ash deposit sediment samples was carried out on powdered unoriented preparations by using a Bruker D8 Advance diffractometer using primary monochromator filtered Cu-K α radiation and LynxEye detector system. Rietveld analysis of XRD patterns was carried out using the Topas code; the relative error of quantification was better than 10% for major phases (content > 5 wt%) and better than 20% for minor phases (content < 5 wt%). The calcium silicate hydrate (C-S-H, in cement notation) phase was modelled via a tobermorite-like structure that provides a rough estimate of this gel-like semicrystalline compound. For putative C-S-H gel the estimated relative error is in the same range with minor phases (i.e. up to 20%).

Pressed pellets were used to determine the chemical composition of selected EPP ash sediment samples by X-ray fluorescence spectroscopy (XRF) using Rigaku Primus II spectrometer. Loss on ignition (LOI) was determined by heating the samples at 950 °C for 2 h. Common phases often present in cement are given in cement notation (Taylor, 1997): C = CaO; S = SiO₂; H = H₂O; A = Al₂O₃; F = Fe₂O₃.

Imaging and chemical analyses of carbon-coated polished aggregates and platinum-coated freshly broken surfaces were carried out with Zeiss EVO 15MA scanning electron microscope equipped with an Oxford X-MAX energy dispersive detector system (EDS) and AZTEC software for element analysis and distribution mapping.

Attenuated Total Reflectance Fourier' Transform Infrared spectroscopy (ATR-FTIR) patterns of selected samples of EPP ash sediments were measured using micro-ATR-accessory attached to Thermo Scientific Nicolet 6700 FT-IR spectrometer. Thermogravimetric analysis (TGA) was carried out using STA 449 F3 Jupiter analyzer in Al₂O₃ crucibles on powdered samples first dried at 70 °C. The samples were heated from 40 °C to 1025 °C at a rate of 10 °C/min in a N₂ flow of 60 ml/min.

Nuclear magnetic resonance ^{29}Si MAS-NMR spectra of selected EPP ash sediment samples were recorded on Bruker AVANCE-II NMR spectrometer at 8.5 T magnet (^{29}Si resonance frequency 71.4 MHz) using single pulse excitation and home-built MAS probe for 10 mm zirconia rotors. The sample was rotated at 5 kHz, the excitation pulse was 7 μs (90°), relaxation delay 100 s, each spectrum is a sum of 800 accumulations. The chemical shifts are given in tetramethylsilane (TMS) scale. Deconvolution of the NMR spectra was performed using combination of Lorentzian and Gaussian line shapes (i.e. Voigt line shape).

The $\delta^{13}\text{C}$ and $\delta^{18}\text{O}$ values of carbonates in 19 EPP ash deposit sediment bulk samples as well as two laboratory experimental sediment samples were measured using Thermo Delta V Advantage continuous flow isotope ratio mass spectrometer. An analytical precision (2σ) of 0.1‰ was determined by repeated analyses of a standard. The dried bulk ash samples were dissolved in 99% H_3PO_4 and the resulting CO_2 gas was analyzed by the spectrometer. The measured isotopic composition is presented as delta notation (δ) in relation to the Vienna Pee Dee Belemnite (V-PDB) standard and expressed in permil (‰). Delta notation is defined as $\delta = [(R_{\text{sample}} - R_{\text{standard}}) / R_{\text{standard}}] * 1000$, where R is the stable isotope ratio of $^{13}\text{C}/^{12}\text{C}$ or $^{18}\text{O}/^{16}\text{O}$.

The equilibrium temperature of the carbonate precipitation was calculated according to (Grossman, 2012; Hays and Grossman, 1991) using equation (1):

$$T = 15.7 - 4.36(\delta^{18}\text{O}_{\text{cal}} - \delta^{18}\text{O}_{\text{water}}) + 0.12(\delta^{18}\text{O}_{\text{cal}} - \delta^{18}\text{O}_{\text{water}})^2, \quad (1)$$

where the $\delta^{18}\text{O}_{\text{cal}}$ values correspond to measured oxygen isotopic composition of calcite relative to V-PDB and $\delta^{18}\text{O}_{\text{water}}$ is the monthly weighted mean Estonian rainfall oxygen isotopic composition of -10.4‰ for the years 1982–85 relative to V-SMOW (Vienna Standard Mean Ocean Water) from Punning et al. (1987). This period corresponds to the peak in oil shale mining and hence ash generation. More recently Stansell et al. (2017) have suggested an average total annual precipitation weighted value of -10.3‰ $\delta^{18}\text{O}_{\text{V-SMOW}}$ for the Estonian area but this causes only a minute variation in calculated values.

The Munsell colour system codes were used for colour definition in 70 EPP ash sediment samples covering the full section of the deposit and three samples from the underlying sediments of the ash deposit. A representation of the Munsell colour codes were converted into digital approximations in the sRGB colour system (Centore, 2013; Geng, 2015).

3. RESULTS AND DISCUSSION

3.1. Composition and long-term diagenesis of hydrated oil shale ash sediments at waste deposits

3.1.1. Chemical and phase composition

The mineral composition of hydrated and partly carbonated ash sediments is characterized by terrigenous phases dominated by relatively heat-resistant silicate minerals, as well as secondary mineral phases formed either during thermal processing or via hydration reactions during deposition, subsequent carbonation and diagenesis (Leben et al., 2019 – PAPER I; Leben et al., 2021 – PAPER III). The content of primary silicate phases ranges from a few percent to over 50 wt%, being mainly characterized by such silicate minerals as quartz, K-feldspar and minor amounts of micas. Carbonates (calcite and vaterite) constitute the main detected secondary minerals, making up an average of 6.6, 25.2 and 18.6 wt% of the material in the EPP ash depository drill core and BPP drill cores No. 5 and 6, respectively. The combined average content of the secondary Ca hydrate-sulphate-silicate phases portlandite, ettringite and thaumasite in three drill cores is 5.1, 5.0 and 4.1 wt%, respectively, but its content can vary considerably. (Fig. 2; Leben et al., 2021 – PAPER III).

The semicrystalline phase composition is characterized by the C-(A)-S-H-type phase trending towards the bottom of the deposit, with estimated values ranging from ca. 20 wt% to more than 60 wt% in the EPP depository drill core and up to 40 wt% in BPP drill core No. 6. However, in BPP drill core No. 5 the C-(A)-S-H phase shows a U-shaped trend from top to bottom, starting from 30–40 wt% and after dropping to 5–10 wt% in the middle part at a depth of 10–17 m increases again to 30–40 wt% in the lower half of the core (Fig. 2).

The chemical composition of the studied EPP ash depository sediments shows a similar variation to the mineral composition (see Fig. 4 in Leben et al., 2019 – PAPER I). The main chemical components CaO and SiO₂ have opposing trends in the cross-section. The average calcium oxide content is 40.9 wt% with a variation of 25.5 to 50.9 wt%. The mean silica content is 19.6 wt% and it varies between 12.5 and 27.6 wt%. Al₂O₃ content ranges from 4.6 to 11.9 wt%. Higher values of Al₂O₃ were detected in surface layers and at depth between 11 to 17 metres. SO₃ content stayed between 2.6 and 9.2 wt%. The content of other elements remains below 5 wt%. The measured loss on ignition (LOI) was rather uniform in samples and did not show significant fluctuations (Fig. 4 in Leben et al., 2019 – PAPER I). The total mass loss at 950°C was between 14.9 and 25.7 wt% with an average value of 17.5 wt%.

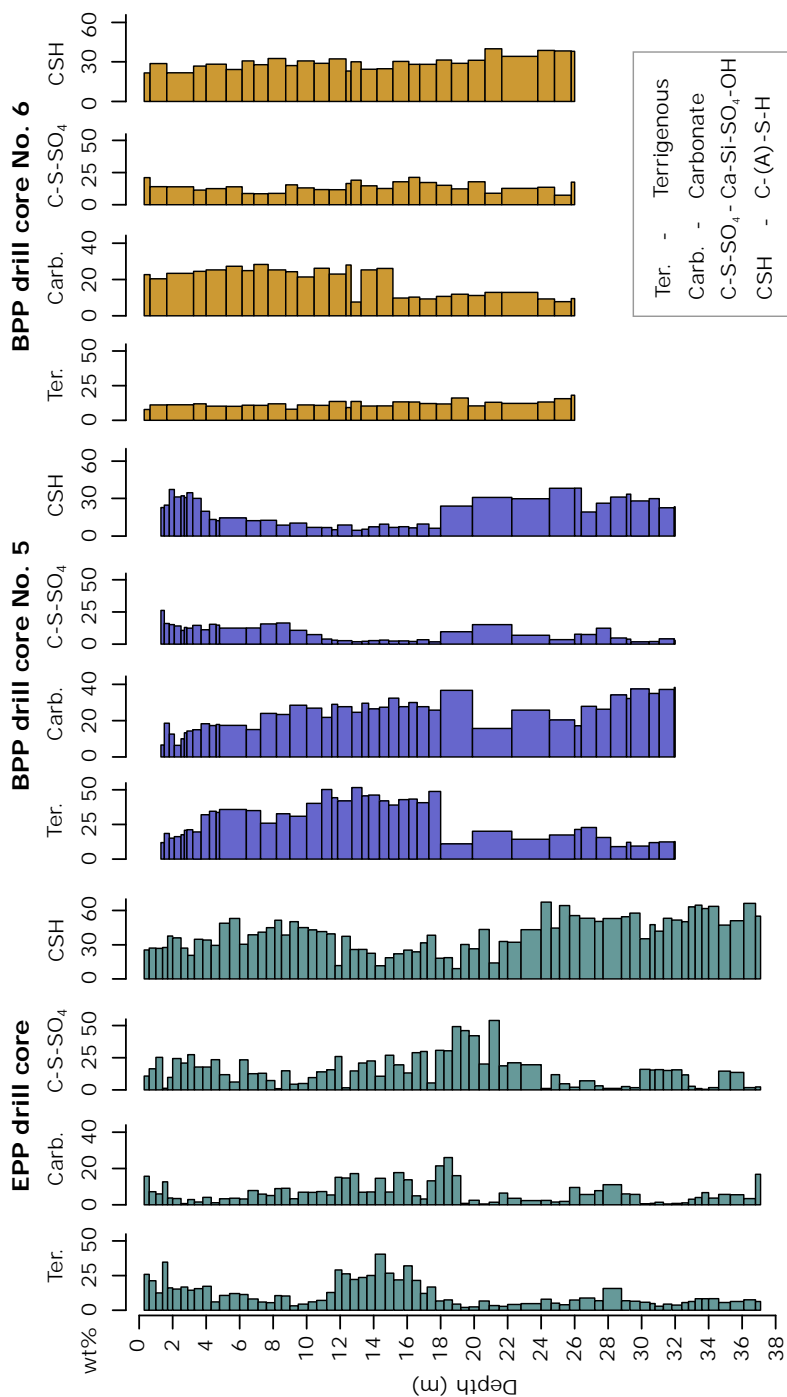


Figure 2. The mineral composition (wt%) of ash sediment drill core samples. Mineral groups legend: Terrigenous = quartz, K-feldspar and mica; carbonate = calcite and vaterite; Ca-Si-SO₄-OH = portlandite, ettringite and thaumasite; C-(A)-S-H = Ca-(Al)-Si-hydrate phase.

A scanning electron microscopy (SEM-EDS) study of EPP ash sediments was undertaken to characterize sediment micromorphology development through ageing of the ash deposit, and to estimate its phase composition (Fig. 3; Leben et al., 2019 – PAPER I). Sediments at shallow depths (<10 m) are relatively porous, composed of Si-Ca-(Al) composition solid spheres or (partially) hollow cenospheres, in a matrix composed of variable grain-size calcite, portlandite and residual terrigenous mineral aggregate (Fig. 3). The size of the spheres ranged from less than 10 μm to greater than 100 μm . Small <5 μm -diameter Fe-rich spheres are commonly dispersed in sediment matrix. The Si-Ca composition of the spheres show limited alteration and dissolution with typically few micron thick leaching zones at the outer perimeter (Fig. 3C).

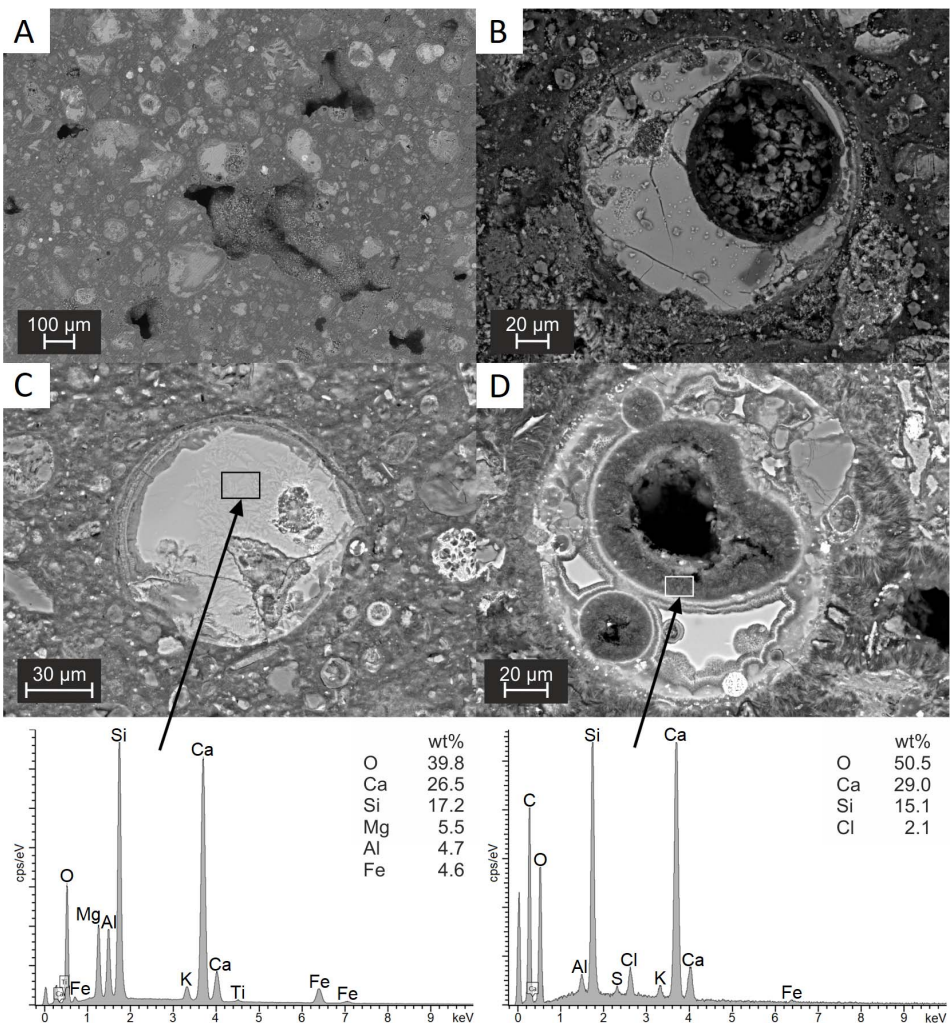


Figure 3. Backscattered electron images of polished sediment at shallow depths. (A) General view of sample from a depth of 2.5 m. (B) Si-Ca-(Al) (ceno-)sphere at 2.5 m depth. (C) Glassy sphere with alteration rim at 10.1 m depth. (D) Recrystallized sphere at 10.1 m depth.

Alteration and recrystallization intensity increase with depth and by 10 m depth the glassy spheres are replaced by flaky-fibrous Ca-Si-hydrate masses (Fig. 3D) and other secondary phases, such as thaumasite and ettringite acicular shape meshes (see Fig. 6 in Leben et al., 2019 – PAPER I). EDS analyses of Ca-Si-hydrate phase show a Ca/Si wt% ratio of about 1.5–2 (Fig. 3 spectra). Semicrystalline masses of C-S-H often show increased Al (additionally K, Mg and Fe), suggesting the formation of more complex forms of hydrate phases, such as C-A-S-H.

ATR-FTIR analyses of selected EPP ash sediment samples were conducted in order to qualitatively support phases assigned in XRD modelling. ATR-FTIR spectra of samples (Fig. 4) from 2.9 m and 22.8 m show a characteristic band around 3642 cm^{-1} that can be assigned to O-H stretching of higher portlandite content (Paiste et al., 2017), which is confirmed by XRD analysis of these samples. Two previously described samples and a sample from 34.0 m show C-O stretching bands around 1450 cm^{-1} in their spectra, indicative of carbonates, while the band at 874 cm^{-1} is due to the out-of-plane bending of carbonate ions (Yu et al., 1999). The band at 960 cm^{-1} is indicative of Si-O stretching vibrations and it can be associated with the presence of Q^2 Si-sites possibly in C-S-H type phases (Paiste et al., 2017; Yu et al., 1999). This band is also present in all spectra but shows growing intensity with sample depth, which is also supported by higher C-S-H-type phase content determined in the lower part of the section by XRD analysis.

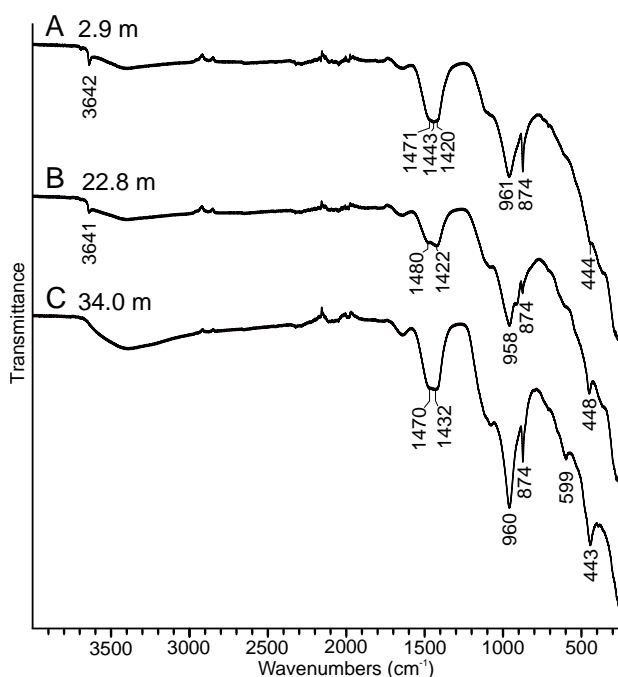


Figure 4. Characteristic ATR-FTIR spectra of EPP ash sediment samples from depths of 2.9 m (A), 22.8 m (B) and 34.0 m (C).

Thermogravimetric analysis (TGA) was carried out to help qualitatively identify portlandite and different hydrate phases, including such X-ray amorphous phases as C-S-H in selected EPP sediment samples (Leben et al., 2019 – PAPER I). However, the multitude and overlapping phases in oil shale ashes make quantitative estimation unreliable (Scrivener et al., 2016). TGA lines with higher mass loss at the lower temperatures of more than 100 °C in samples from the depth of 18.7 and 20.9 m (Fig. 5) can be associated with the higher composition of hydrate phases ettringite and thaumasite in these samples (Scrivener et al., 2016). Characteristic sharp mass loss at around 400–450 °C is due to the dehydroxylation of $\text{Ca}(\text{OH})_2$ (Alarcon-Ruiz et al., 2005; Scrivener et al., 2016; Ukrainczyk et al., 2006). The mass losses at around 600–700 °C, most prominent in the samples from the depths of 2.9, 18.7, 20.9 and 22.8 m, can be assigned to CO_2 loss, mainly from carbonates (Frías et al., 2016; Scrivener et al., 2016). This is best observed in the sample from a depth of 18.7 m with a two-stage mass loss, starting from around 500 °C, with the second step starting around 750 °C. This mass loss, however, can also be attributed to amorphous CaCO_3 or thaumasite (Alarcon-Ruiz et al., 2005; Scrivener et al., 2016). The identification of C-S-H-type phases is complicated in TGA analysis, but a mass loss of ~18% without clear peaks seen in the sample from the depth of 34.0 m can be tentatively attributed to C-S-H (Scrivener et al., 2016; Zhang and Ye, 2012) and other possible X-ray amorphous phases.

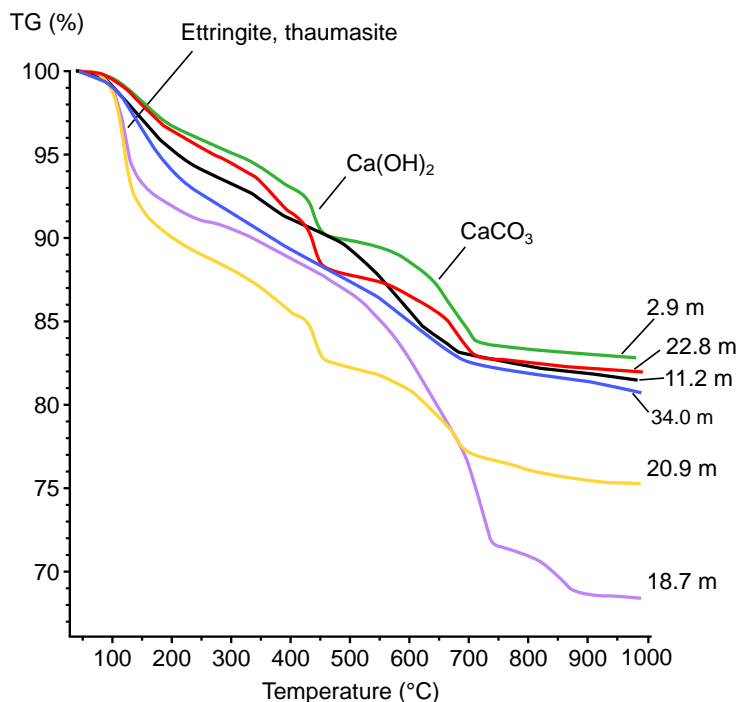


Figure 5. TGA patterns of selected EPP ash sediment samples from different depths of the ash deposit.

NMR spectra of selected EPP deposit ash samples were analyzed to characterize primary and secondary silicate phases, including semicrystalline C-S-H. The recorded spectra (Fig. 6) show the detection of Q^0 Si-sites associated with C_2S (belite) in two forms, β - C_2S and γ - C_2S , marked by the two peaks with chemical shifts around -71 and -73 ppm, respectively. The peaks at around -79 , -81.9 , -83.5 , -85 and -89 ppm mark the different Si-tetrahedra positions, Q^1 , $Q^2(1Al)$, Q^2_b (bridging), Q^2_p (pairing) and Q^3 , respectively, related typically to C-S-H type phases. An amorphous glassy phase can also be interpreted as a shallow wide peak at around -91 to -95 ppm. The peak at around -107 ppm (Q^4) is attributed to quartz, while the peak at -67 ppm on spectrum 20.9 m can be putatively interpreted as nesosilicate $CaMgSiO_4$ (Chang et al., 2016; Magi et al., 1984; Myers et al., 2015; Paiste et al., 2017; Richardson, 1999).

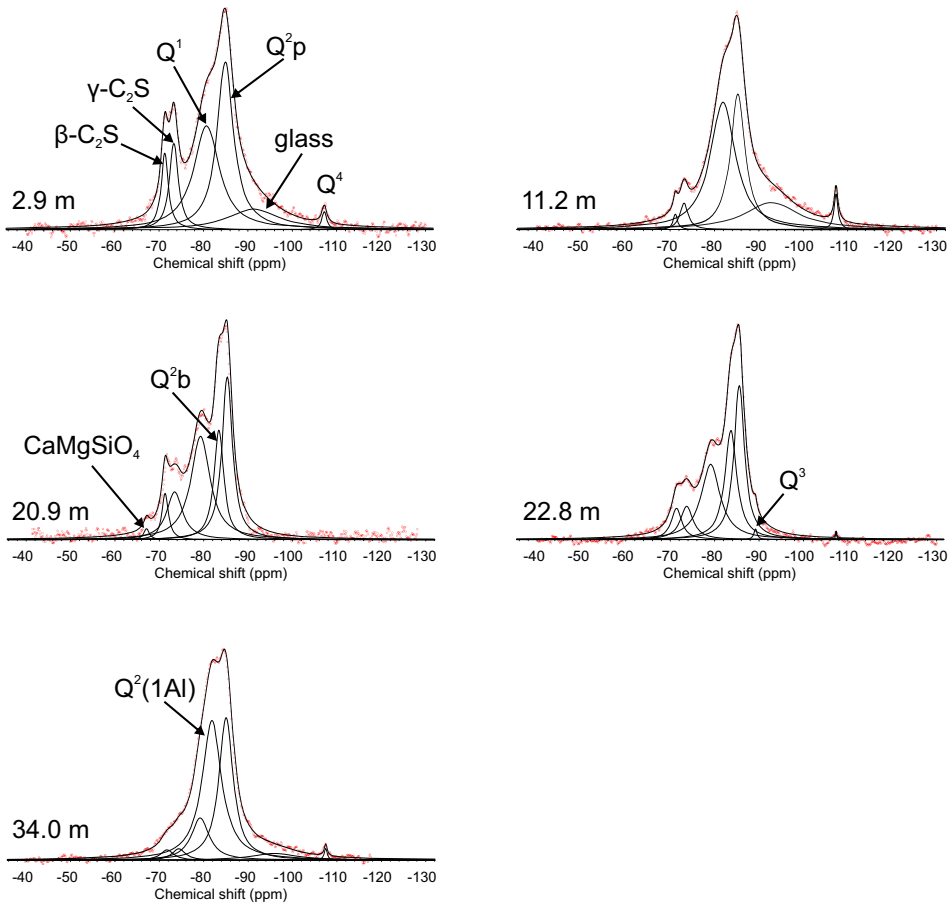


Figure 6. NMR spectra of studied EPP ash deposit sediment samples.

The NMR spectra show significant changes along the depth profile. Wide peaks representing amorphous glass are clearly distinguishable and prominent in two most shallowly-buried samples (2.9 and 11.2 m), but these peaks diminish with increasing depth, indicating the dissolution and recrystallization of glass phase over time. A similar trend is evident in Q^0 peaks, showing a relative decrease in intensity to nearly disappearing in the deepest/oldest sample, which is consequently accompanied by a relative increase in different Si-sites of the chained silicates (Q^1 , $Q^2_b/Q^2(1Al)$ and Q^2_p). A distinct peak at -89.1 ppm corresponding to a Q^3 site was detected only in one sample from a depth of 22.8 m. The deepest sample studied, from a depth of 34.0 m, shows an intense peak at -81.8 ppm that can be assigned to representing $Q^2(1Al)$ units. This indicates Al-tetrahedra substitution in the Si-chains, which is supported by the increasing Al content in possible C-(A)-S-H-type phases, detected by SEM-EDS analyses in the lower part of the ash deposit. Quartz peak (Q^4) at -107 ppm was detected in most of the studied samples, but it was nearly absent in the middle part of the succession.

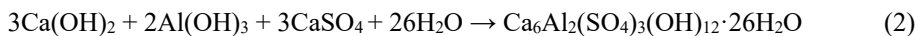
3.1.2. Ash sediment diagenesis

The diagenesis of Ca-rich ash sediments has been studied mostly at laboratory scale, suggesting that the carbonation of metastable Ca-phases is a dominant process (Liira et al., 2009; Mötlep et al., 2010; Velts et al., 2013). However, the current study benefits from the new valuable data obtained by the drilling program conducted through the entire thickness of the deposit. It shows that the *in-situ* mineralization of Ca-rich ash sediment is dominated by alkali-activated recrystallization of either initial terrigenous or secondary silicate phases. The final product of this long-term alteration is a semicrystalline C-S-H type phase along with ettringite and thaumasite, whereas the carbonation is significantly subdued in deeper parts of the deposit.

The composition of ash sediment in waste depositories is firstly dictated by the composition of ash forming in boilers and its sequential hydration reactions during and after the deposition (Mötlep et al., 2010). The ash from both power plants is rich in reactive secondary Ca-phases, such as lime (CaO_{free}) and anhydrite, as well as secondary Ca/Mg-silicates. These phases form during the thermal decomposition of carbonate minerals (calcite and dolomite) present in raw oil shale. The reactions start thereafter, between CaO_{free} (and free MgO) and silicates, as well as flue gases, mainly SO_2 (e.g., Bityukova et al., 2010). Lime slaking (reaction 1) and the formation of portlandite start already during the transportation and deposition of ash:



This is followed by the dissolution of anhydrite and subsequent reactions involving dissolved Ca, sulphate and Al, producing ettringite type phases (reaction 2):



Earlier studies (e.g., Liira et al., 2009) have shown that ettringite forms over a period of about two weeks, followed by the formation of hydrocalumite type phase ($\text{Ca}_2\text{Al}(\text{OH})_7 \cdot 3\text{H}_2\text{O}$) and/or gypsum ($\text{CaSO}_4 \cdot 2\text{H}_2\text{O}$) (Liira et al., 2009; Möttelep et al., 2010). In the long term a key role in ash recrystallization is played by the hydration of secondary Ca-silicate minerals such as belite (C_2S). Based on NMR spectra, C_2S phase exists in two polymorphs: $\beta\text{-C}_2\text{S}$ which forms at 500–680 °C and $\gamma\text{-C}_2\text{S}$ which forms below 500 °C (Taylor, 1997). Belite hydration is one of the possible sources of C-S-H type phases, but this reaction can also lead to a secondary formation of portlandite in the ash sediments (Chen et al., 2004) by reaction (3):



The other probable source of C-S-H type phases is the recrystallization of aluminosilicates and the dissolution of amorphous glassy phases in naturally alkaline conditions mimicking alkali activation (Duxson et al., 2007; Paiste et al., 2017; Yip et al., 2005). C-S-H content, as indicated by XRD pattern modelling with a tobermorite-like structure, shows an increase with depth (from about 25% to over 60%) with an exception in the middle part of the deposit. The same trends are supported by the NMR results, which show that the peaks assigned to glassy amorphous silicates and belite are higher in shallow layers and diminished in favour of different Si-units of C-S-H type phases in deeper layers. A similar trend in increasing amorphous phase content was already noticed by Möttelep et al. (2010), but its nature was not discussed.

In laboratory conditions, about 30% of $\beta\text{-C}_2\text{S}$ reacts in 28 days and 90% in 1 year (Taylor, 1997). On the other hand, the alkali activation of aluminosilicate raw materials, the formation of C-S-H gel like phases and the development of strength can last for several years (de Vargas et al., 2014). The gradual increase of the C-S-H-like phase and the recrystallization of the mineral matrix in studied ash material continuously deposited for almost 50 years suggests a slow dissolution of primary crystalline and glassy silicate phases, which is probably further inhibited by limited hydraulic conductivity between cemented ash layers.

In terms of alkali activation, the Ca-rich ash can be viewed as a one-part alkali-activated material in a broad sense. As opposed to conventional two-part activation, where typically concentrated aqueous solution of alkali hydroxide or silicate solution and solid raw material are mixed, in one-part mixtures the dry mixture containing reactive phases is only mixed with water (Luukkonen et al., 2018). In carbonate rich fossil fuel combustion ash, the hydration of lime (CaO_{free}) provides alkaline medium for activation reactions that most likely

progress in a typical alkali activation manner: ion exchange – hydrolysis – mineral/glass structure network breakdown and the release of Si and Al which undergo further speciation, gelation, reorganization, and polymerization (Duxson et al., 2007; Luukkonen et al., 2018; Matalkah et al., 2017). Similar reactions releasing Si and Al in alkaline environment resulting in gel formation are observed in geopolymer mixtures treated with NaOH (Rattanasak and Chindaprasirt, 2009).

Luukkonen et al. (2018) have pointed out that the release rate and availability of Si and Al from solid silica sources used in one-part mixes are lower than in two-part alkali-activated materials. A similarity between the Ca-rich ash and one-part alkali-activated materials is the formation of semicrystalline C-S-H and probably of C-A-S-H gel, which are typically observed in calcium-rich one-part alkali-activated systems along with other secondary hydration products, such as portlandite, brucite, katoite, hydrocalumite and ettringite-thaumasite (Kim et al., 2013).

The SEM-EDS analyses of studied Ca-rich drill core materials show that most of the material identified as C-S-H type phase exhibit mostly a high C/S ratio of around 2, but a somewhat lower ratio (around 1.5) in the deeper parts of the section. Taylor (Taylor, 1997) has proposed two different possible formulae of C-S-H by eliminating bridging tetrahedra from tobermorite and jennite: $\text{Ca}_5\text{H}_2\text{Si}_4\text{O}_{16} \cdot 8\text{H}_2\text{O}$ (C/S = 1.25) and $\text{Ca}_9\text{H}_2\text{Si}_4\text{O}_{16}(\text{OH})_8 \cdot 6\text{H}_2\text{O}$ (C/S = 2.2), respectively. Considering this, the upper section C-S-H phase corresponds to type II C-S-H (Chen et al., 2004; García et al., 2009), while the micromorphology of the C-S-H masses in lower part of the section suggests type I (C/S around 1.5) (Stutzman, 2001; Taylor, 1997). This change might indicate further recrystallization of C-S-H, e.g. carbonation (García-Lodeiro et al., 2012), although Richardson (2004) and Richardson and Cabrera (2000) have reported that the mean C/S ratio of C-S-H in neat C_3S or OPC pastes does not vary with age. Still, the majority of non “synthetic” C-S-H type phases that form from $\beta\text{-C}_2\text{S}$, called C-S-H gel, are less ordered and exhibit a ratio of 1.7–1.8 (Chen et al., 2004), probably being the most common products forming in OS ashes. Alternatively, the variation in C/S ratio can be caused by initial variability in ash composition (Ca, Si and Al), fraction size, and environmental conditions (temperature and water availability).

The polymerisation and development of longer chains in C-S-H type phases, formed in Ca-rich OS ash over time can be characterized by calculating their mean chain lengths (MCL), using the equation (4) provided by Richardson (1999) and the equation (5) incorporating cross-linking Q^3 units (in the case of sample from 22.8 m depth) by Myers et al. (2013):

$$\overline{\text{CL}} = \frac{2}{\left(\frac{\text{Q}^1}{\text{Q}^1 + \text{Q}^2(0\text{Al}) + \frac{3}{2}\text{Q}^2(1\text{Al})} \right)} \quad (4)$$

$$\text{MCL}_{[\text{C}]} = \frac{4[\text{Q}^1 + \text{Q}^2 + \text{Q}^2(1\text{Al}) + \text{Q}^3 + 2\text{Q}^3(1\text{Al})]}{\text{Q}^1} \quad (5)$$

The calculated chain lengths (Table 1) show the formation of longer silicate chains with increasing depth, indicated by a relative decrease in Q^1 chain-end sites, an increase in Q^2 pairing and bridging units, as well as an increase in Q^3 units in the bottom layers (in the sample from a depth of 22.8 m) and $Q^2(1Al)$ units (from 34.0 m) tied to Al-substitution in silicate chains. This supports the hypothesis of slow recrystallisation of amorphous glassy phases and simple Ca-silicates in favour of longer chain-structured C-S-H-type phases.

Table 1. Calculated mean chain lengths (MCL) in studied samples

Depth, m	2.9	11.2	20.9	22.8	34.0
MCL	5.2	4.1	8.3	18.5	18.6

NMR analyses show the presence of $Q^2(1Al)$ units, which indicate in some cases Al-tetrahedra substitution of Si-tetrahedra. Al substitution of Si is supported by SEM-EDS analyses, which show higher Al content in C-S-H-type phases, particularly in a sample from a depth of 33.6 m. This suggests the formation of C-A-S-H-type phases in the deepest and oldest layers of the deposit. The notion that the development of longer products cross-linked with Q^3 -units is caused by the incorporation of Al is also supported by Myers et al. (2015), who have shown that cross-linking Q^3 formation is promoted by Al presence.

The occurrence of portlandite in higher amounts at different levels throughout the section can be of both primary or secondary origin. First of all, the primary portlandite forms by the fast slacking of lime that starts to react in open air with atmospheric CO_2 , forming a stable Ca-carbonate phase. Uibu and Kuusik (2014) have explained the preservation of portlandite in ash sediment by the formation of carbonated crust on the freshly deposited ash layers, inhibiting CO_2 diffusion and complete carbonation of deposited ash. Sediment ponds are episodically filled with ash slurry that is allowed to set. Next layers are added in the same manner, creating a layered ash deposit. The slow or incomplete carbonation of portlandite can also help retain the stability of some mineral phases (e.g., ettringite) due to high pH. However, secondary portlandite can also form as a side product of C-S-H type phase precipitation from the hydration of C_2S (Chen et al., 2004). Assuming secondary formation of portlandite, its higher concentrations could be an indication of higher initial C_2S content.

It is particularly interesting that ettringite and thaumasite show an opposite trend with C-S-H phase in EPP ash sediments (Leben et al., 2019 – PAPER I). Ettringite is a typical secondary mineral in OS ash deposits (Mötlep et al., 2010), which forms early during hydration when Al-bearing phases/glass react with water and $CaSO_4$. Thaumasite, however, can form at the expense of ettringite in the presence of dissolved silica and inorganic carbon, or by the carbonation and dissolution of C-S-H under low temperature conditions (under 15 °C, optimal 5 °C), high pH (10.5–13) and abundance of water (Bensted, 1999; Crammond, 2003; Hartshorn et al., 1999; Sear, 2006; Zhou et al., 2006). Thaumasite shows elevated content in the middle part of the section (depths between 13–21 m), where there is also a drop in C-S-H content (Fig. 3; Leben et al., 2019 – PAPER I).

Crammond (2003) suggests that thaumasite will continue to form if the aforementioned requirements are fulfilled and a source of SiO_2 , CO_3^{2-} and SO_4^{2-} ions is available. As thaumasite has low solubility in these conditions, all other potential sources of ions (including C-S-H) will gradually dissolve to keep the pore solution at an equilibrium. Ettringite, with a similar crystalline structure to thaumasite, shows a similar increase in the same section of the deposit and generally follows a trend with thaumasite. It has also been reported that the two phases can form solid solutions (Barnett et al., 2000; Torres et al., 2004). Experimental studies of ettringite-thaumasite solid solution formation suggest that ettringite acts as a nucleating agent or catalyst for thaumasite formation (Taylor, 1997). These trends suggest that C-S-H phase initially formed in this interval is undergoing dissolution and replacement with ettringite-thaumasite. Permeability and/or hydrogeological properties, as well as the structural integrity (fracturing) of the ash sediments are yet to be determined, but this alteration can be related to the differences in ash layer permeability due to the differences in ash sediment composition and/or grain size, or fracturing and enhanced water flow as a result of this.

Nevertheless, the general composition of the ash deposited in sedimentary ponds has remained the same during the entire period of power plant exploitation since 1969, except for the uppermost interval at about 5–8 m, where, in addition to the ash from pulverized combustion boilers, the waste from circulating fluidized bed combustion boilers commissioned in 2004 has been co-deposited. However, the fuel used in the power plant has remained the same over time (calcareous oil shale). Since 1980 lesser amounts of oil retorting ash have also been co-deposited on the fields, but this has not affected the ash composition significantly. There can be grain-size separation during the filling of ash ponds with the ash-water slurry. However, the observed sizes of glassy spherules and cenospheres does not show variation throughout the section, suggesting that grain-size separation does not control the sediment properties, at least not significantly. Given the present state of knowledge, the fracturing of sediment heap and the enhanced water flow can be forwarded as the possible cause of this zone.

In general, alkali activation type processes with the aging of Ca-rich ash sediments and the formation of a binding hydration product C-S-H phase will increase the mechanical strength of the ash sediment depositories in time and decrease their permeability by reducing pore size. Therefore, it ensures the long-term stability of the waste deposits, enhancing their reclamation possibility as construction sites.

In the coal industry, older high-temperature pulverized combustion (PC) boilers are gradually being replaced with more environmentally friendly low-temperature circulating fluidized bed combustion (CFB) boilers. However, as is the case with various CFB ashes around the world (Gazdič et al., 2017), these ashes generally display less favourable properties for producing construction materials. Lowered pozzolanic properties are caused by relatively lower combustion temperatures, which lead to lower amounts of reactive phases in ash, specifically, lower CaO and glassy amorphous material content (e.g., Gazdič et al., 2017). Our results show that all deposited oil shale ash waste types have the potential to achieve better mechanical properties with the formation of C-S-H-type phases

due to the long-term alkali-activation induced by alkaline waters circulating in the deposits. No additional alkali or silicate additive substances are required if the reaction period is long enough to allow the dissolution and recrystallisation of various crystalline and glassy silicate phases. This means that waste, which has been conditioned under alkaline conditions for decades, can be reused as an aggregate in road construction and building. Alternatively, given their activation in self-sustaining alkaline conditions, the CFB ashes with low reactivity can be used in applications where strength gain comparable with OPC mortars is not required e.g. for the backfilling of open cast quarries and underground mines. Apart from its high alkalinity, Estonian oil shale ash is low in potential toxic heavy metals; the content of Cd, Cr, Pb and Zn is 5–10 times lower than in typical municipal waste incineration fly ashes and lower than or comparable to average values for coal fly ash (Blinova et al., 2012; Zhao et al., 2018). Therefore, the reuse of solidified ash material is not limited in these applications.

3.2. Carbonation of Ca-rich ash waste

3.2.1. Carbonate carbon and oxygen stable isotope composition of ash waste

All analyzed sediment samples show negative $\delta^{13}\text{C}$ and $\delta^{18}\text{O}$ values relative to the V-PDB scale (Leben et al., 2020 – PAPER II). The $\delta^{13}\text{C}$ values varied from -11.9‰ to -22.9‰ for ash waste deposit samples and $\delta^{13}\text{C}$ values in laboratory experiment samples were -23.2‰ and -24.3‰ after two weeks and three months, respectively (Fig. 7; Table 2). The $\delta^{18}\text{O}$ values varied between -7.9‰ and -15.1‰ for the waste deposit sediments, and -12.0‰ and -14.2‰ for laboratory experiment samples after two weeks and three months, respectively. There is no clear statistically significant correlation between C- and O-isotope values (Fig. 7).

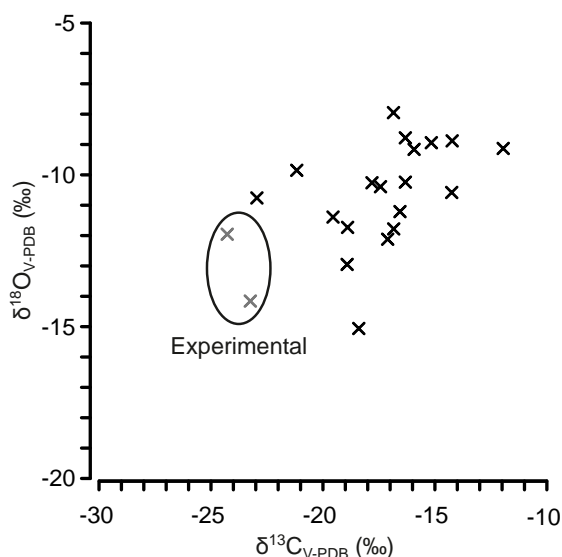


Figure 7. Carbon and oxygen stable isotope composition of ash sediments.

Table 2. The stable isotope composition and calculated equilibrium temperatures of EPP ash sediments. Experimental cemented ash samples- Exp (hardening time, weeks/months).

Depth (m)	$\delta^{13}\text{C}_{\text{V-PDB}} (\text{‰})$	$\delta^{18}\text{O}_{\text{V-PDB}} (\text{‰})$	Temperature ($^{\circ}\text{C}$)
0.45	-11.95	-9.13	10.36
1.85	-19.55	-11.39	20.13
3.55	-17.11	-12.12	23.55
5.70	-18.92	-12.95	27.60
7.85	-14.25	-10.58	16.49
9.80	-16.56	-11.21	19.31
11.90	-14.23	-8.88	9.35
13.85	-16.85	-7.95	5.74
16.05	-16.32	-8.78	8.95
17.95	-18.40	-15.06	38.62
20.00	-16.84	-11.78	21.95
22.40	-16.32	-10.24	15.01
24.85	-18.90	-11.73	21.71
27.00	-17.43	-10.39	15.66
29.05	-22.95	-10.76	17.29
31.05	-15.16	-8.94	9.59
33.00	-15.93	-9.16	10.48
34.95	-17.81	-10.26	15.09
38.25	-21.17	-9.85	13.34
Exp(2 w)	-23.24	-14.16	33.77
Exp(3 m)	-24.28	-11.96	22.77

The colour of the sediments in the studied section varies from white-pale grey (Munsell colour code – Gley 1 9/N) to dark grey (Gley 1 4/N) (Leben et al., 2020 – PAPER II; Fig. 8; supplementary data table online at <https://doi.org/10.15152/GEO.491>). Darker layers correspond to a higher share of oil retorting ash. The darkest layers with the highest estimated oil retorting ash content occur in the uppermost 2 m and at around 12 m depth. Layers with an estimated medium to low oil retort ash content are located at around 7–9, 13–18 and 22 m. The lowest darker layers occur between 25 and 28 m depths, likely indicating the period around the first deposition of oil retorting ash in the deposit in the 1980s. Layers of lighter-coloured ash with no apparent oil retorting ash content make up the most of the deposit, occurring around 2–7, 9–12, 17–21 and 22–25 m depths; and from 28 m onwards to the bottom of the deposit at 38 m depth. The very bottom of the ash deposit lies above the brown-coloured (code 10 YR 5/3) compressed peat layer and the sand- and clay-rich layers below it.

Some covariation between sample colour and mineral composition has been reported by Leben et al., (2019 – PAPER I). In general, grey-coloured samples with a higher estimated oil retorting ash content also display a higher terrigenous mineral content. Pale beige coloured combustion ash layers correspond to an elevated secondary Ca-mineral (portlandite) content. However, a clear correlation between sample colouration and mineral or chemical composition could not be established.

The measured $\delta^{13}\text{C}$ value of carbonates formed in the ash sediment is remarkably negative compared with typical natural carbonate sediments. The carbonate (calcite) precipitating in equilibrium with atmospheric CO_2 should have a $\delta^{13}\text{C}$ value of around 0‰. Present-day $\delta^{13}\text{C}$ values of atmospheric CO_2 shifted from *ca.* -7.5‰ in the late 1970s to -8.3‰ by 2015 (Keeling et al., 2017), which would result in a shift of about -1‰ to carbonate $\delta^{13}\text{C}$ values. Typically, negative stable carbon isotope values are considered to signal the involvement of CO_2 of organic origin, for example from microbial activity (Campbell et al., 2003; Whiticar, 1999). In this sense the strongly ^{13}C depleted carbonate isotope values in the ash depository at Eesti Power Plant seemingly point towards the involvement of CO_2 derived from bacterial degradation of some residual organics. The atmospheric $\delta^{13}\text{C}$ value is around -8‰, with an equilibrium fractionation between atmospheric CO_2 and calcite of +9.6‰ (Emrich et al., 1970), and the CO_2 derived from the degradation of organic matter has a $\delta^{13}\text{C}$ value of *ca.* -30‰. Hence, assuming a simple mixing and mass balance between these two CO_2 reservoirs would lead to the oil shale ash carbonate $\delta^{13}\text{C}$ values varying from -11.9‰ to -22.9‰, this would denote the contribution of organics-derived light CO_2 to the total CO_2 pool in the range of 50–90%.

However, the carbonate isotope fractionation in natural environments is also sensitive to the pH of the environment where carbonate minerals are precipitated because of pH dependence on isotope fractionation between carbon species (e.g., Swart, 2015). The correlation between carbon isotope composition and the varying pH in precipitating calcite has previously been brought out by Dietzel et al. (1992), showing that carbonate precipitated at higher pH has a more negative isotopic composition than the calcite precipitated under neutral pH conditions.

The diagenetic transformation of Ca-rich ash sediments in highly alkaline conditions can be compared to past and present natural alkaline environments, where negative stable carbon isotope fractionation in authigenic carbonate phases has been described (e.g., Arp et al., 2016, 2013; Leleu et al., 2016). Nevertheless, in most cases the natural highly alkaline water bodies are soda lakes (for example Lake Bogoria, Lonar Lake, Mono Lake and others), which have a comparatively low Ca^{2+} and Mg^{2+} content. The main carbonate minerals forming in these environments are usually Na-based (Grant, 2006). Carbonate precipitation rates in these lakes are very low, being associated with high evaporation and low outflow rates, ensuring a stable high pH and, often, elevated salinity. However, the $\delta^{13}\text{C}$ values of Na-carbonates forming in these lakes can also be positive (Anoop et al., 2013; Grant, 2006).

There are alkaline water bodies, often related to hydrothermal activity, where the cation composition of alkaline water is dominated by dissolved Ca and Mg species. These water bodies are more similar to oil shale ash depository pond environments and processes. They can be compared to natural alkaline environment in a former lake basin inside the Ries meteorite crater in southern Germany, formed 14.59 ± 0.20 Ma ago (Buchner et al., 2010). After the impact, the crater depression was filled with an isolated lake, where lacustrine sediments accumulated over a long period of time during different stages of lake development with highly varying environmental conditions, resulting in carbonate sediments with a wide range of isotopic compositions (Arp et al., 2013). The $\delta^{13}\text{C}$ values of carbonate precipitates in this alkaline lake and associated hot water spring travertine deposits (and hydrothermal vein calcite) are in the range of +4‰ to –8‰ (Arp et al., 2016). These are much higher isotopic values than the $\delta^{13}\text{C}$ values of –14‰ to –23‰ recorded in the oil shale ash deposit.

The negative $\delta^{13}\text{C}$ values seen in this study are more similar to those of travertines formed at hyper-alkaline springs in the Oman ophiolite massif (Clark et al., 1992; Leleu et al., 2016). The Oman system is characterized by Ca-rich highly alkaline groundwaters (pH up to 11.9), where carbonate deposits have $\delta^{13}\text{C}$ values as negative as –22.8‰. In this setting, the $\text{Ca}(\text{OH})_2$ -type hyper-alkaline groundwater depleted in dissolved inorganic carbon (DIC) and enriched in Ca leads to the fast precipitation of calcite, when mixing with inorganic carbon-rich surface water and on diffusion of atmospheric CO_2 (Clark et al., 1992).

Under hyper-alkaline conditions, the carbonate system is far from equilibrium, the highly negative non-equilibrium fractionation of stable isotopes in carbonates being controlled by aqueous kinetic effects during the hydroxylation of CO_2 (Clark et al., 1992). Clark et al. (1992) have suggested that the diffusion of atmospheric CO_2 occurs rapidly with respect to aqueous reactions, reaching equilibrium conditions between aqueous and gaseous CO_2 with the enrichment factor of 1‰ for ^{13}C in $\text{CO}_{2(\text{aq})}$. They concluded that a significant 15.56‰ depletion of $\delta^{13}\text{C}$ values in the carbonate phases precipitating in alkaline conditions is the result of the lower activation energy of ^{12}C –O bonding (compared to ^{13}C –O) on the hydroxylation reaction of $\text{CO}_{2(\text{aq})}$ with OH^- producing HCO_3^- (equation 6):



Bicarbonate becomes hydrolysed to CO_3^{2-} in alkaline conditions (equation 7), which is the dominant species at high pH values above 10 (associated with a depletion of *ca.* –0.4‰ with respect to the ^{13}C at 25 °C):



On the other hand, Dietzel et al. (1992) have suggested that the reported depletions in ^{13}C of carbonates are due to additional kinetic effects, caused by the different diffusion rates of gaseous $^{13}\text{CO}_2$ and $^{12}\text{CO}_2$ as well as the hydroxylation rates of dissolved aqueous CO_2 . The latter view was also supported by the study of Leleu

et al. (2016). Similar hyper-alkaline conditions occur during oil shale ash deposition and diagenesis. The water–ash slurry, initially depleted in dissolved carbon and enriched in Ca due to the fast exothermic slaking of free CaO as well as the subsequent dissolution of portlandite, starts the rapid precipitation of calcite on contact with atmospheric CO₂. It is therefore highly likely that the low $\delta^{13}\text{C}$ values of carbon bound to authigenic carbonate in oil shale ash deposits are not of organic origin. Instead, the negative $\delta^{13}\text{C}$ values are caused by the kinetic fractionation effects on both the diffusion of CO_{2(g)} and the hydroxylation of CO_{2(aq)} in the highly alkaline, bicarbonate-depleted and relatively low-temperature conditions in oil shale deposits. Similar processes have been demonstrated during the carbonation of municipal waste ash, where carbonate sediments form in a fluid oversaturated with Ca²⁺ ions. The higher the activity of the ions in the fluid, the more negative the $\delta^{13}\text{C}$ values of calcite become (Fléhoc et al., 2006). Such conditions are achieved when fluid comes into contact with portlandite or cement phases, such as C-S-H gel, which can raise the pH of the fluid to over 12.5 (Létolle et al., 1992). The same kinetic fractionation process has also been observed in carbonate crusts and stalactites formed on old concrete structures, as a result of the chemical weathering of Ca-rich phases, such as C-S-H gel (Krishnamurthy et al., 2003; Macleod et al., 1991).

In the presence of portlandite, the kinetic fractionation takes place upon the diffusion of CO₂ molecules into the water film surrounding Ca(OH)₂. The molecules containing light carbon (¹²C) isotopes are preferred for carbonate formation and as a result the precipitating CaCO₃ is about –10‰ lower than gaseous CO₂ (Fléhoc et al., 2006). Adding this to the atmospheric CO₂ $\delta^{13}\text{C}$ value of around –8‰, the resulting hypothetical $\delta^{13}\text{C}$ value of the Ca-carbonate precipitating under such conditions would be –18‰. This fits with the average measured $\delta^{13}\text{C}$ value of –17.2‰ in oil shale ash sediments in this study.

The large variation in the $\delta^{13}\text{C}$ values of carbonate in oil shale ash deposits, when compared to equilibrium values, can be explained by the incorporation of residual carbonate (calcite), potentially present in bottom ash fraction. Alternatively, the variation can be explained by the calcite precipitation at the later stages of carbonation where pH values drop below 9 and thus approach equilibrium state. The more negative values hint at additional fractionation in different kinetic steps (Clark et al., 1992; Létolle et al., 1992). This results in a total maximum fractionation of $-15.5 \pm 1.5\text{‰}$ during the hydroxylation of aqueous CO₂, and a final carbonate $\delta^{13}\text{C}$ value of –23‰. This agrees with the minimum measured values of –21‰ to –22.95‰ in oil shale ash deposits and particularly in the laboratory experiment, where the $\delta^{13}\text{C}$ values were even slightly more negative than in the oil shale ash plateau.

The variation in ambient temperature can influence the diffusion during kinetic fractionation, adding to the extent of the fractionation on gaseous CO₂. This view is supported by the weak covariation between carbonate $\delta^{13}\text{C}$ and $\delta^{18}\text{O}$ values (Fig. 7). In general, the lowest $\delta^{13}\text{C}$ carbon isotope values also display the most ¹⁸O depleted isotope composition. This would imply that higher temperatures during carbonation (as referred from oxygen isotopic composition) in fact

lead to more depleted ^{13}C isotope composition in carbonates (Fig. 8). However, such direct comparison from oxygen isotopic composition to environmental temperatures cannot be made in this system as it is far from the equilibrium state. This is further exemplified by the large variation in calculated temperatures for the ash deposit sediments, ranging from 5.7 to 38.6 °C, with an average value of 16.5 °C, and particularly by the temperatures 22.8 and 33.8 °C of experimental samples after two weeks and three months of curing, respectively (Table 2). The laboratory experiment was performed at room temperature, varying between 20 and 22 °C for the whole experiment period. After two weeks of curing, the temperature calculated by using oxygen isotope fractionation thermometry agrees with the ambient temperature in the laboratory. However, after three months the calculated temperature significantly deviates from the ambient conditions in the laboratory.

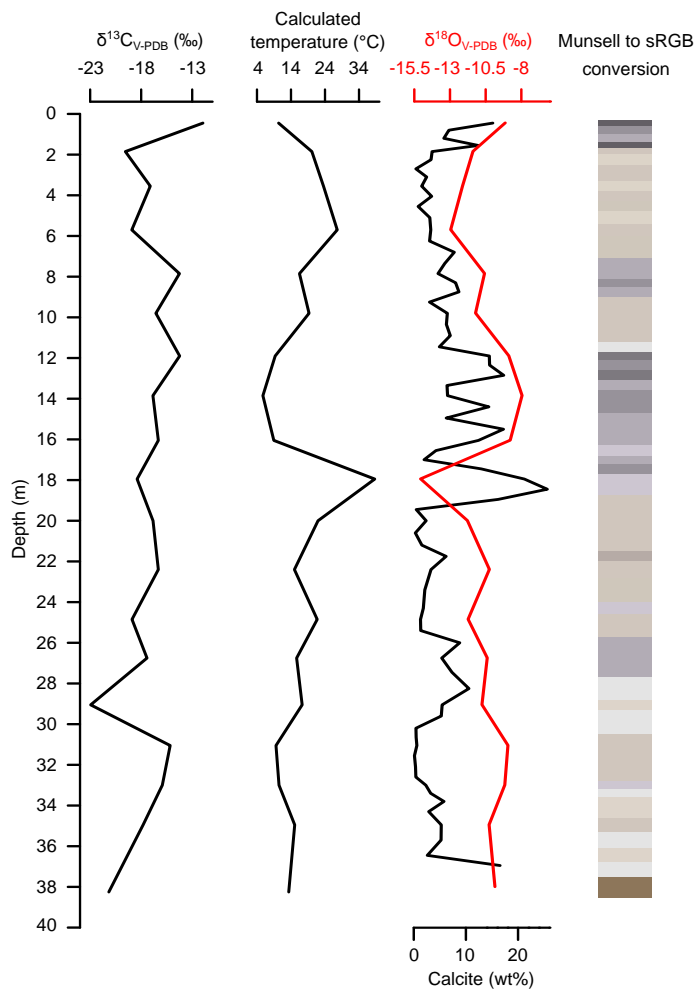


Figure. 8. Calculated equilibrium temperatures and Munsell colouration of samples, compared to the isotopic composition of selected EPP ash sediment samples.

First of all, this depletion in the oxygen isotopic composition of authigenic calcite can be mainly attributed to the reaction of $\text{CO}_{2(\text{aq})}$ with strongly $^{18}\text{O}_{\text{depleted}}$ OH^- (Clark et al., 1992), but it also signals strong kinetic effects on the oxygen isotopic composition of the authigenic carbonate precipitating in oil shale ash deposits. Furthermore, earlier studies of carbonates formed under DIC-depleted hyper-alkaline conditions (Leleu et al., 2016; Teboul et al., 2016) show a similar positive trend between negative $\delta^{13}\text{C}$ and $\delta^{18}\text{O}$ values, reflecting non-equilibrium isotopic shifts in dissolved inorganic carbon. This is due to progressive calcite precipitation (and CO_2 degassing in some environments), making the temperatures calculated based on temperature-controlled equilibrium fractionation on the formation of carbonates unreliable (Mickler et al., 2006). It is possible that during the deposition of large amounts of ash sediment, fast carbonation will locally deplete the solution reservoir of CO_3^{2-} carrying light oxygen, whereas the diffusion, hydration and the hydroxylation reactions of CO_2 will not be fast enough to ensure isotopic equilibrium.

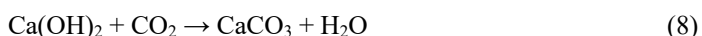
As discussed above, the highly negative $\delta^{13}\text{C}$ values of carbonates (-11.95‰ to -22.95‰) in ash sediment samples, which are typically associated with an organic origin of carbon, are likely of inorganic origin and result from kinetic fractionation effects in this unusually alkaline environment. This can further be tested by the possible covariation of organic-rich retorting ash beds and the isotopic composition of authigenic carbonate. Darker-coloured SHC oil retorting ash has a residual organic content of up to 3% (Talviste et al., 2013). Part of the carbon bound in carbonates may originate from the aerobic decomposition of this organic material, or original oil shale, leading to the more negative $\delta^{13}\text{C}$ composition of the carbonate. However, no correlation between darker layers and the most negative $\delta^{13}\text{C}$ values could be made. Furthermore, the highest $\delta^{13}\text{C}$ value (-11.9‰ , depth 0.45 m) was found in a dark sample and the lowest value (-22.9‰ , depth 29.05 m) was measured in a white ash sample (Fig. 8). The isotopic value of the stratigraphically topmost samples can be skewed by the contribution from residual carbonate from CFBC ash. However, in deeper parts of the deposit, high-temperature PC ashes dominate without or with minimal residual carbonate content.

3.2.2. Mineral carbonation potential of Ca-rich ash waste

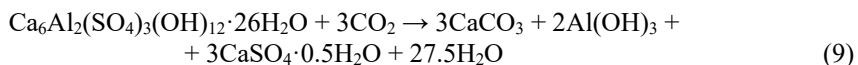
Mineral carbonation is one of the promising means to control atmospheric CO_2 balance by providing substrate and process for CO_2 sink. In terms of composition, Ca-rich oil shale ash sediment is comparable to other natural alkaline metal bearing minerals (silicates), widely available in igneous and metamorphic rocks (Leben et al., 2021 – PAPER III). Weathering products of rocks bearing these minerals are known for their capacity to bind atmospheric CO_2 . This process can be utilized in manmade applications, but it requires energy-intensive processing in order to transform these minerals into a carbon dioxide binding substrate (IPCC, 2005; O'Connor et al., 2005; Sanna et al., 2014). However, there are examples of

using natural geological processes (e.g., Magbitang and Lamorena, 2016) and ultramafic mine tailings (Oskierski et al., 2013; Turvey et al., 2018) as carbon sinks, which do not require significant external energy input. However, the industrial-scale applicability of these processes has yet to be determined. A faster and less energy-dependent substitute for natural silicates for carbon mineralization would be metal oxides (CaO, MgO)-bearing industrial waste, e.g. Ca-rich oil shale ash deposits in Estonia. These wastes are often related to the same point sources of CO₂ emission and are dumped in close proximity, which make the waste a promising substrate for direct or indirect carbon capture.

Carbon dioxide sequestration in oil shale ash deposits relies mostly on the carbonation of portlandite (8) which mainly forms by the slaking of lime and/or the hydration of Ca-silicate minerals present in raw ash:



Additional CO₂ binding capacity in hydrated oil shale ash can be provided by the decomposition and carbonation of ettringite (9), secondary Ca-silicate phases (10) producing Ca-sulphate, Al-hydroxide and/or silica, along with calcium carbonate phases (Nishikawa et al., 1992):



The presence of thaumasite (Ca₃Si(OH)₆(CO₃)(SO₄)·12H₂O) in oil shale ash sediment (up to 30 wt%) also indicates that at least some of the CO₂ is bound by this mineral. This has previously not been taken into account when estimating the CO₂ sequestration capacity in oil shale ash waste. Thaumasite can form at the expense of ettringite in the presence of dissolved silica and dissolved inorganic carbon. Alternatively, it can form as a result of the carbonation of C-S-H gel-like phase and the consumption of portlandite (Hartshorn et al., 1999; Zhou et al., 2006), providing an additional CO₂ sink in ash sediments.

Under laboratory conditions, the carbonation of portlandite, the main CO₂ binding phase in oil shale ash, takes place over several weeks or months (Kuusik et al., 2004). Geochemical modelling and laboratory scale studies of oil shale ash carbonation (Kuusik et al., 2002; Trikkel et al., 2010; Uibu et al., 2010, 2009, 2008; Uibu and Kuusik, 2014; Velts et al., 2011) show that CO₂ sequestration in ash material is viable and that PC oil shale ash has a theoretical CO₂ capture capacity of 350–500 kg of CO₂ per one tonne of ash. 30–50% of this potential is based on free lime. However, in agreement with findings of Mõtlep et al. (2010) and Leben et al. (2019 – PAPER I), our results show that abundant portlandite is still found at deep levels throughout the plateau sediment succession. This implies retarded carbonation, which is most probably the result of inhibited transport of CO₂ dissolved in the ash transport water and rainwater infiltrating into the ash deposit.

Laboratory studies and theoretical calculations have overestimated the extent of carbonation within the ash deposit. This is because the actual composition of ash sediment inside the ash deposits or, more importantly, the pathways of ash diagenesis have remained unknown. This is the first time that the actual material from the whole succession of the deposit is available to assess CO₂ binding capacity. Firstly, it is necessary to account for the residual carbonate content in fresh ash. In older PC boilers, almost all carbonates are thermally decomposed (decomposition extent reaches 98%), but the carbonate decomposition extent in lower temperature CFBC boilers can vary between 47–96% in different ash fractions (Kuusik et al., 2005). The average residual primary calcite content in PC ash is estimated to be 5.16% of crystalline phases (Table 3), calculated using the calcite content and the proportion of different ash fractions in fresh ash with data by Bityukova et al. (2010) and Konist et al. (2013). Given that CFBC ash with a lower extent of decarbonation has been deposited in ash plateaus only during the last decade, causing PC ash to prevail in ash deposits, this calculated average calcite content estimate can be used to describe the share of primary carbonate in average ash stream.

Table 3. The average primary calcite content in the crystalline fraction of different PC ash fractions (Bityukova et al., 2010; Konist et al., 2013).

Ash fraction	Calcite, wt%	Proportion of ash, %	Calcite in total ash prior to storage, wt%
Furnace	6.4	42.1	2.69
Super heater	3.3	3.7	0.12
Economizer	4.4	4.7	0.21
Cyclone separator	4.2	14.5	0.61
I el. precipitator	4.3	28.3	1.22
II el. precipitator	4.7	5.6	0.26
III el. precipitator	4.2	1.1	0.05
Total:			5.16

Abbreviation: el. – electric.

In raw ash the content of amorphous glassy material typically not detected in X-ray diffraction analysis is estimated at 29 wt% on average (Mötlep et al., 2010). This means that the content of primary carbonate is ca. 30 wt% less, making up 3.6 wt% of bulk material on average, including crystalline and amorphous phases. Similarly, the assessment of carbonation extent by using X-ray diffraction data requires the consideration of the share of amorphous C-(A)-S-H-type phase when calculating general mass balance. The content of secondary Ca-carbonate minerals (calcite and vaterite) formed by CO₂ uptake in ash sediments varies widely, ranging between 0–35%. The respective amount of CO₂ bound to ash sediment ranges from 0 to 153 kg of CO₂ per tonne of the sediment. There is high

variability between the analyzed drill cores in the average content of bound CO₂: it is 1.6, 8.9 and 6.6 wt% for the EPP drill core and BPP drill cores No. 5 and 6, respectively. In addition to Ca-carbonates, the Ca-silicate-sulphate mineral thaumasite also binds a fraction of carbon dioxide. The CO₂ in thaumasite can either be of atmospheric origin or originate from the dissolution of carbonates (Aguilera et al., 2003; Dyer, 2014). Calcite and vaterite are stable phases in the pH range of 12–13, which is characteristic of the water in contact with OS ash (Pihu, et al., 2019). This suggests that most of the CO₂ likely originates from the atmospheric CO₂, rather than the dissolution of carbon bearing phases. Carbon dioxide bound to thaumasite ranges from 0 to 22.8 kg of CO₂ per tonne of ash sediment with an average of 3 kg/t (Fig. 9; see Supplementary Table 1 in Leben et al., 2021 – PAPER III).

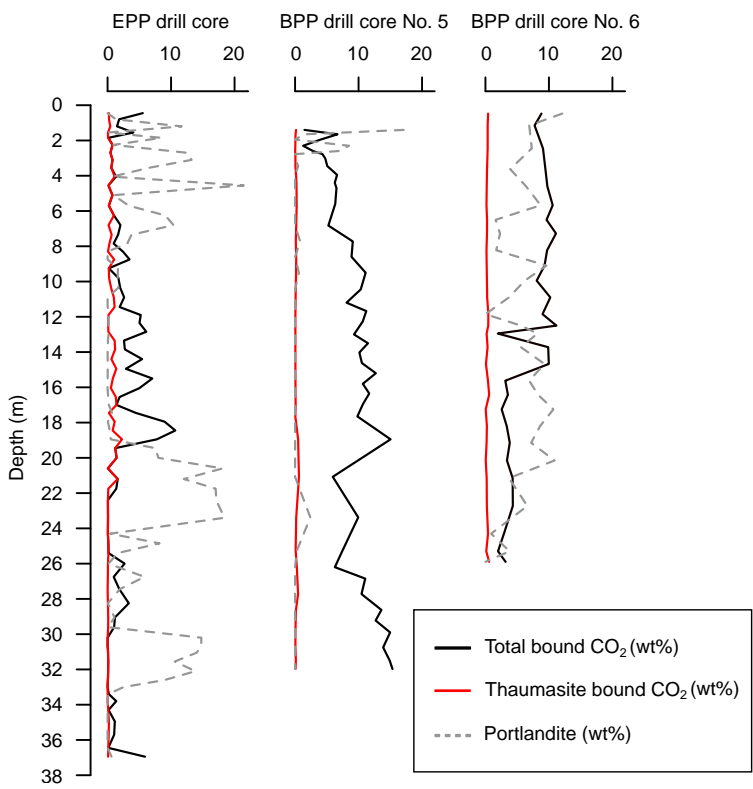


Figure. 9. Carbon dioxide binding rate in studied ash sediment samples.

These results show that Ca-rich ash sediments deposited over a long period of time display highly variable CO₂ binding rates, which remain far below the previously reported values. The average CO₂ sequestration capacity in carbonates is only 4.8 wt% or 48 kg per tonne of ash sediment, when considering the composition of all three drill core sections. As the water-binding capacity of dry ash is 0.15 m³ per tonne on average, this being mainly consumed to form portlandite, gypsum, ettringite and various other hydrates (Liira et al., 2009), this means that

ca. 41 kg of CO₂ is bound per tonne in ash sediment on dry ash basis. Adding the CO₂ bound in thaumasite, the total average amount of bound CO₂ rises to 4.3 wt% or 43 kg per tonne of dry ash or 51 kg/tonne of ash sediment. This suggests that thaumasite accounts for about 6% of the total bound CO₂ on average. Furthermore, in several intervals, particularly in the drill core succession of EPP ash depository, the estimated content of CO₂ bound in ash sediment was close to or below the level of CO₂ assumed to be included in average estimated primary calcite composition, which indicates a zero net uptake of CO₂ by ash sediments.

The high variation in CO₂ bound in the mineral form of the ash sediment is firstly caused by the compositional heterogeneity of ash sediments and secondly by the inhibited CO₂ transport into the sediment pile. The long-term variability in CO₂ uptake is partially caused by the seasonal and historical changes in the production capacity of the plants. Namely, after the fall of the Soviet Union there was a large drop in ash production, decreasing from 15 million to 7–9 million tonnes per year. In 2019 production came down to ca. 4–5 million tonnes per year, due to the significantly reduced oil shale firing caused by unfavourable market conditions under current carbon dioxide trade policies. The ash deposits are sequentially built up, layer by layer, by the deposition of the ash-water slurry in the temporary ponds on top of plateau-like ash deposits (Pihu et al., 2019, 2012). Earlier studies have revealed a highly variable layered structure of ash deposits (Arro et al., 2003), the thickness of a typical layer ranging from 0.2 to > 1 m (Pihu et al., 2012). The layers that show lower CO₂ binding rates can likely be associated with higher ash production periods, meaning more rapid burial and a shorter and more inhibited contact with CO₂. For example, this is true for layers in the lower section of the EPP drill core at the depths of 20 to 25 meters (Fig. 9). Also, because of grain size separation in the settling of the ash-water slurry along about a 1000+ m long flow-path, the coarse-grained fractions of bottom ash are deposited at the inlet of the slurry with progressively finer particles, mainly represented by the fly ash fractions, settling further along the flow path. This causes the lateral variation in ash composition (Pihu et al., 2012). In addition, the position of the slurry inlet and the flow path of braided streams are changed at each filling step, causing further grain size and compositional spatial variation. Arro et al. (2003) have shown that coarse-grained bottom ash fractions form loose and porous ash sediment beds, while fine-grained ash forms nearly impermeable and hard layers with a transverse filtration module as low as $0.15 \cdot 10^{-9}$ m/s. It is evident that such dense layers significantly reduce both water and CO₂ transport from the top of the plateau down to its deeper parts. According to Konist et al. (2016), the binding of CO₂ mostly takes place during ash-water transport and within the surface (layers) of deposits, but it stops when the contact with ambient air is lost. However, it is possible that CO₂ transport following ash deposition occurs more readily through steep (ca. 30 degrees) 30–40 m high walls of the depositories, preferentially via coarse-grained ash beds composed of hydrated bottom ash particles (Fig. 10). Furthermore, the material at the sides of the plateaus is thoroughly mixed during the dam building process, which further facilitates CO₂ uptake. As a result, following the initial phase during deposition,

carbonation mainly occurs at the sides of ash deposits and the full potential of CO₂ sequestration in hydrated ash deposits is not achieved. This is well evident from the survival of Ca-hydroxide (portlandite) throughout the ash sediment successions (Fig. 9). Although some portlandite can also be of secondary origin, formed during alkali-activation and the formation of C-S-H-type phases from Ca-silicates, its presence nevertheless hints at limited CO₂ transport and carbonation processes inside the ash plateau sediments. In addition, the carbonation of portlandite at the edges of the ash deposits causes effective pore space closure, further inhibiting this process inside the ash piles.

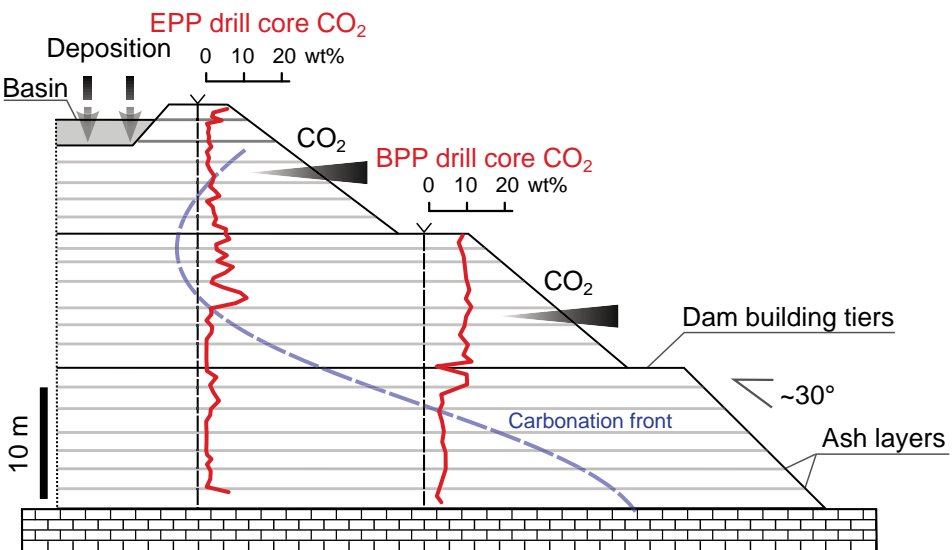


Figure 10. The conceptual (not-to-scale) scheme of CO₂ uptake in the ash deposits. The carbonation line is drawn based on the presence of portlandite in sediment mineralogy.

These results show that under natural conditions the full CO₂ binding capacity of ash sediments has not been reached during the last 50 years. If the calculated binding rate (48 kg/tonne of ash sediment) is applied to the recent annual average ash production of 7.2 Mt, and with CO₂ emissions being at 11.3 Mt (Eesti Energia, 2019), we find that on average only about 3.06% of released CO₂ is bound by oil shale ash waste in the long term. When taking thaumasite into consideration and calculating the amount of CO₂ based on dry ash binding capacity (43 kg/t), an average of 2.74% of emissions is bound to ash sediment annually. This is well below the previously assessed lower end values of 4% CO₂ bound to ash depositories (Kuusik et al., 2001). Given that ash production rates and the respective CO₂ emissions were more than twice as high in the mid-1980s, and that the studied drill cores were situated at the edges of the ash plateaus with a more advanced carbonation rate, it can be suggested that the overall binding capacity has most probably been overestimated by as much as an order of magnitude.

Assuming that the lower half of the deepest drill core in the ash depository at EPP represents the composition of ash sediments inside the ash pile away from the walls, less than 1% of CO₂ emission has been bound by ash sediments so far. Nevertheless, Uibu and Kuusik (2014) have demonstrated a high CO₂ sequestration capacity of oil shale ash that is potentially achievable by the *in-situ* carbonation of ash sediment deposits. For instance, this can be achieved by constructing a network of drill holes through ash deposits, connected to the flue gases emitted by the nearby powerplants, forcing accelerated *in-situ* carbonation. In addition to the carbonation of the available portlandite, the *in-situ* carbonation of ash deposits will lead to an extensive Ca-carbonate formation at the expense of all Ca-containing phases, including ettringite, thaumasite and C-S-H gel. While portlandite and ettringite are prone to full carbonation already at atmospheric CO₂ partial pressures, the level of C-S-H carbonation is dependent on the concentration of CO₂ (Hyvert et al., 2010; Nishikawa et al., 1992). It has been shown that C-S-H with an initial Ca/Si ratio of about 1.2 can become almost entirely carbonated in a laboratory under exposed conditions in seven days, forming ca. 80 wt% calcite and 15 wt% silica gel (Suzuki et al., 1985). Furthermore, Wu and Ye (2016) have shown that nearly all C-S-H phases can be fully decomposed to CaCO₃ and silica gel by accelerated carbonation at a CO₂ partial pressure of 0.03 atm after three days, while phases with a higher Ca/Si ratio are more resistant to carbonation. According to Leben et al. (2019 – PAPER I) the Ca/Si ratio of the C-S-H-like phase in ash sediments ranges from 1.5 to 2. They also showed that it is likely more resistant to carbonation.

The average content of portlandite, ettringite and the C-S-H type phases in ash sediment samples is 5, 4.9 and 31.8 wt%, respectively. The full carbonation of portlandite, ettringite and the 80% calcite formation from C-S-H phase would lead to an increase in the average CO₂ content of ash sediment by 3, 0.8 and 11.2 wt%, respectively. This would increase the sediment's potential CO₂ binding capacity by 150 kg/t, resulting in a total of ca. 200 kg/t. In addition, it is possible that at increased CO₂ partial pressures in the flue gases and by using captured CO₂ stream, other Ca and Mg phases such as thaumasite and minor phases such as Ca- and Ca/Mg-silicates, Ca-aluminates, periclase (MgO) and Mg-hydroxide would also contribute to carbonation, further enhancing the CO₂ binding capacity of oil shale ash sediment.

4. CONCLUSIONS

This thesis investigated the long-term diagenesis, composition and stability of Ca-rich oil shale ash waste sediments by analyzing the drill core material, which describes ash sediment piles formed over nearly 50 years at the largest oil shale power plants and oil retorts in Estonia. The carbon and oxygen stable isotopic composition of oil shale ash sediments in the ash waste deposit was studied to decipher the carbonation process and to reveal the main source of the CO₂ bound in authigenic carbonate minerals formed after deposition. The long-term CO₂ sequestration capacity of Ca-rich oil shale ash sediments under natural conditions was assessed by analyzing drill core material taken from EPP and BPP ash waste deposits, containing more than 300 million tonnes of ash. The main conclusions of this thesis are:

- 1) Semicrystalline C-S-H and possibly C-A-S-H type phases gradually form over long periods of time in the naturally highly alkaline conditions of ash sediment deposits. The source of these phases is the slow dissolution and recrystallization of primary crystalline and glassy silicate phases. The content of C-S-H type phases increases from about 25% near the surface to over 60% near the bottom layers. ²⁹Si NMR analyses show the formation of more complex-structured C-A-S-H phases in the bottom layers, suggesting continuous diagenetic recrystallization of silicate phases. The formation of C-S-H and possibly C-A-S-H type phases ensure the increase in mechanical strength and long-term coherence of the deposits.
- 2) The late formation of ettringite-thaumasite and partial dissolution of C-S-H in zones of enhanced permeability, as seen in the EPP drill core data, can cause the deterioration of mechanical properties and possible failure of the deposits. Further research is required to understand the controlling mechanisms behind the thaumasite formation at the expense of C-S-H type phases, in order to look for countermeasures to its formation.
- 3) The stable isotope composition of authigenic carbonate is characterized by $\delta^{13}\text{C}_{\text{V-PDB}}$ values between -12‰ and -24‰ and $\delta^{18}\text{O}_{\text{V-PDB}}$ between -8‰ and -15‰. The non-equilibrium fractionation effects in hyper-alkaline conditions and limited CO₂ transport into the sediments cause the low $\delta^{13}\text{C}$ carbon isotope values of ash sediments. This is because the molecules of CO₂ containing lighter ¹²C isotopes are preferred on diffusion into the water film surrounding Ca(OH)₂ during carbonation.
- 4) Non-equilibrium effects, likely due to the local depletion of lighter isotopic CO₃²⁻ during carbonation, are also responsible for ¹⁸O depleted oxygen isotopic values. Thus, the stable oxygen isotopic composition cannot reliably be used to estimate the equilibrium temperature of the solution during the carbonate formation in oil shale ash deposit sediments.
- 5) Deposited ash material shows high compositional variability, with the average carbonate-bound CO₂ content varying between 1.6 and 8.9 wt% in different drill cores. On average, the CO₂ binding rate of oil shale ash

sediment deposited in waste depositories was found to be 51 kg per tonne, which includes the Ca-silicate thaumasite that accounts for about 6% of the total bound carbon dioxide. This is ca. 5 to 6 times less than the estimated binding capacity in laboratory-scale experiments.

- 6) The carbonation of portlandite, which has been considered to be the main process governing the diagenetic transformation of Ca-rich ash sediments, is inhibited within ash deposits after the deposition and burial of ash slurry. Under natural conditions, carbonate formation is significantly hindered by limited CO₂ transport, with only the outer perimeter of ash deposits having likely been partially carbonated. This suggests that the internal part of the ash pile is left largely unreacted, as evidenced by the preservation of Ca-hydroxide in the deeper parts of the sections. At current production rates, however, ash is deposited in lower rates than before. This will likely increase the CO₂ binding rate of the deposit in the surface layers due to its prolonged contact with atmospheric CO₂.
- 7) The CO₂ sequestration potential of ash sediments can be increased by *in-situ* carbonation, using flue gases from the nearby power plants. Assuming full carbonation of the major phases, i.e. portlandite, ettringite and C-S-H, the average CO₂ binding capacity of ash can be increased by about 150 kg/t, resulting in a total estimation of ca. 200 kg/t.

Oil shale ash sediments display various physical, chemical and mineralogical characteristics after deposition, as well as long-term transformation in the natural environment. These properties depend on the chemical and mineralogical content of used oil shale, processing methods and temperature (combustion or retorting), the fraction size of ash (fly ash to bottom ash), the age of the sediment, seasonal fluctuations in temperature and precipitation, and even the location of the sediment within the ash deposit. Changes in these properties can widely affect the mechanical strength and the mineral carbonation potential of the sediments. Therefore, further investigation should be conducted in the central parts of the deposits in order to confirm the presented trends and assessments, particularly regarding the potential for CO₂ sequestration in carbonate minerals.

REFERENCES

- Aguilera, J., Martínez-Ramírez, S., Pajares-Colomo, I., Blanco-Varela, M.T., 2003. Formation of thaumasite in carbonated mortars. *Cem. Concr. Compos., Thaumasite in Cementitious Materials* 25, 991–996.
[https://doi.org/10.1016/S0958-9465\(03\)00121-5](https://doi.org/10.1016/S0958-9465(03)00121-5)
- Alarcon-Ruiz, L., Platret, G., Massieu, E., Ehrlicher, A., 2005. The use of thermal analysis in assessing the effect of temperature on a cement paste. *Cem. Concr. Res.* 35, 609–613. <https://doi.org/10.1016/j.cemconres.2004.06.015>
- Aminu, M.D., Nabavi, S.A., Rochelle, C.A., Manovic, V., 2017. A review of developments in carbon dioxide storage. *Appl. Energy* 208, 1389–1419.
<https://doi.org/10.1016/j.apenergy.2017.09.015>
- Anoop, A., Prasad, S., Plessen, B., Basavaiah, N., Gaye, B., Naumann, R., Menzel, P., Weise, S., Brauer, A., 2013. Palaeoenvironmental implications of evaporative gaylussite crystals from Lonar Lake, central India. *J. Quat. Sci.* 28, 349–359.
<https://doi.org/10.1002/jqs.2625>
- Arp, G., Hansen, B.T., Pack, A., Reimer, A., Schmidt, B.C., Simon, K., Jung, D., 2016. The soda lake – mesosaline halite lake transition in the Ries impact crater basin (drilling Löpsingen 2012, Miocene, southern Germany). *Facies* 63, 20.
<https://doi.org/10.1007/s10347-016-0483-7>
- Arp, G., Kolečka, C., Simon, K., Karius, V., Nolte, N., Hansen, B.T., 2013. New evidence for persistent impact-generated hydrothermal activity in the Miocene Ries impact structure, Germany. *Meteorit. Planet. Sci.* 48, 2491–2516.
<https://doi.org/10.1111/maps.12235>
- Arro, H., Prikk, A., Pihu, T., 2006. Calculation of CO₂ emission from CFB boilers of oil shale power plants. *Oil Shale* 23, 356–365.
- Arro, H., Prikk, A., Pihu, T., 2003. Reducing the environmental impact of Baltic Power Plant ash fields. *Oil Shale* 20, 375–382.
- Barnett, S.J., Adam, C.D., Jackson, A.R.W., 2000. Solid solutions between ettringite, Ca₆Al₂(SO₄)₃(OH)₁₂·26H₂O, and thaumasite, Ca₃SiSO₄CO₃(OH)₆·12H₂O. *J. Mater. Sci.* 35, 4109–4114. <https://doi.org/10.1023/A:1004898623884>
- Bauert, H., Kattai, V., 1997. Kukersite oil shale, in: *Geology and Mineral Resources of Estonia/ Raukas A., Teedumae A. (Eds.). Estonian Academy Publishers, Tallinn*, pp. 313–327.
- Bensted, J., 1999. Thaumasite — background and nature in deterioration of cements, mortars and concretes. *Cem. Concr. Compos., Portland Limestone Cements* 21, 117–121. [https://doi.org/10.1016/S0958-9465\(97\)00076-0](https://doi.org/10.1016/S0958-9465(97)00076-0)
- Bitjukova, L., Mötlep, R., Kirsimäe, K., 2010. Composition of oil shale ashes from pulverized firing and circulating fluidized-bed boiler in Narva Thermal Power Plants, Estonia. *Oil Shale* 27, 339–353. <https://doi.org/10.3176/oil.2010.4.07>
- Blinova, I., Bitjukova, L., Kasemets, K., Ivask, A., Käkinen, A., Kurvet, I., Bondarenko, O., Kanarbik, L., Sihtmäe, M., Aruoja, V., Schvede, H., Kahru, A., 2012. Environmental hazard of oil shale combustion fly ash. *J. Hazard. Mater.* 229–230, 192–200. <https://doi.org/10.1016/j.jhazmat.2012.05.095>
- Bobicki, E.R., Liu, Q., Xu, Z., Zeng, H., 2012. Carbon capture and storage using alkaline industrial wastes. *Prog. Energy Combust. Sci.* 38, 302–320.
<https://doi.org/10.1016/j.pecs.2011.11.002>
- Buchner, E., Schwarz, W.H., Schmieder, M., Trieloff, M., 2010. Establishing a 14.6 ± 0.2 Ma age for the Nördlinger Ries impact (Germany)—A prime example for concordant

- isotopic ages from various dating materials. *Meteorit. Planet. Sci.* 45, 662–674. <https://doi.org/10.1111/j.1945-5100.2010.01046.x>
- Bui, M., Adjiman, C.S., Bardow, A., Anthony, E.J., Boston, A., Brown, S., Fennell, P.S., Fuss, S., Galindo, A., Hackett, L.A., Hallett, J.P., Herzog, H.J., Jackson, G., Kemper, J., Krevor, S., Maitland, G.C., Matuszewski, M., Metcalfe, I.S., Petit, C., Puxty, G., Reimer, J., Reiner, D.M., Rubin, E.S., Scott, S.A., Shah, N., Smit, B., Trusler, J.P.M., Webley, P., Wilcox, J., Dowell, N.M., 2018. Carbon capture and storage (CCS): the way forward. *Energy Environ. Sci.* 11, 1062–1176. <https://doi.org/10.1039/C7EE02342A>
- Campbell, B.J., Stein, J.L., Cary, S.C., 2003. Evidence of Chemolithoautotrophy in the Bacterial Community Associated with *Alvinella pompejana*, a Hydrothermal Vent Polychaete. *Appl. Environ. Microbiol.* 69, 5070–5078. <https://doi.org/10.1128/AEM.69.9.5070-5078.2003>
- Centore, P., 2013. Conversions Between the Munsell and sRGB Colour Systems. Unpublished 64.
- Chang, J., Fang, Y., Shang, X., 2016. The role of β -C2S and γ -C2S in carbon capture and strength development. *Mater. Struct.* 49, 4417–4424. <https://doi.org/10.1617/s11527-016-0797-5>
- Chen, J.J., Thomas, J.J., Taylor, H.F.W., Jennings, H.M., 2004. Solubility and structure of calcium silicate hydrate. *Cem. Concr. Res.* 34, 1499–1519. <https://doi.org/10.1016/j.cemconres.2004.04.034>
- Clark, I.D., Fontes, J.-C., Fritz, P., 1992. Stable isotope disequilibria in travertine from high pH waters: Laboratory investigations and field observations from Oman. *Geochim. Cosmochim. Acta* 56, 2041–2050. [https://doi.org/10.1016/0016-7037\(92\)90328-G](https://doi.org/10.1016/0016-7037(92)90328-G)
- Crammond, N.J., 2003. The thaumasite form of sulfate attack in the UK. *Cem. Concr. Compos.* 25, 809–818. [https://doi.org/10.1016/S0958-9465\(03\)00106-9](https://doi.org/10.1016/S0958-9465(03)00106-9)
- Crippa, M., Oreggioni, G., Guizzardi, D., Muntean, M., Schaaf, E., Lo Vullo, E., Solazzo, E., Monforti-Ferrario, F., Olivier, J., Vignati, E., 2019. Fossil CO₂ and GHG emissions of all world countries (EUR – Scientific and Technical Research Reports). Publications Office of the European Union, Luxembourg, pp. 246.
- de Vargas, A.S., Dal Molin, D.C.C., Masuero, Á.B., Vilela, A.C.F., Castro-Gomes, J., de Gutierrez, R.M., 2014. Strength development of alkali-activated fly ash produced with combined NaOH and Ca(OH)₂ activators. *Cem. Concr. Compos.* 53, 341–349. <https://doi.org/10.1016/j.cemconcomp.2014.06.012>
- Dietzel, M., Usdowski, E., Hoefs, J., 1992. Chemical and ¹³C/¹²C- and ¹⁸O/¹⁶O-isotope evolution of alkaline drainage waters and the precipitation of calcite. *Appl. Geochem.* 7, 177–184. [https://doi.org/10.1016/0883-2927\(92\)90035-2](https://doi.org/10.1016/0883-2927(92)90035-2)
- Dindi, A., Quang, D.V., Vega, L.F., Nashef, E., Abu-Zahra, M.R.M., 2019. Applications of fly ash for CO₂ capture, utilization, and storage. *Journal of CO₂ Utilization* 29, 82–102. <https://doi.org/10.1016/j.jcou.2018.11.011>
- Duxson, P., Fernández-Jiménez, A., Provis, J.L., Lukey, G.C., Palomo, A., Deventer, J.S.J. van, 2007. Geopolymer technology: the current state of the art. *J. Mater. Sci.* 42, 2917–2933. <https://doi.org/10.1007/s10853-006-0637-z>
- Dyer, T., 2014. Concrete Durability. CRC Press. <https://doi.org/10.1201/b16793>
- Eesti Energia, 2019. Annual Report 2019. Environmental Report. https://www.energia.ee/-/doc/8644186/ettevotte/aastaaruanne/pdf/EE_AA_2019_ENG.pdf (Accessed 13.05.20).

- Elering, 2014. Estonian long-term power scenarios.
<https://elering.ee/sites/default/files/attachments/Estonian-Long-term-Energy-Scenarios.pdf> (Accessed 13.05.20).
- Emrich, K., Ehhalt, D.H., Vogel, J.C., 1970. Carbon isotope fractionation during the precipitation of calcium carbonate. *Earth Planet. Sci. Lett.* 8, 363–371.
[https://doi.org/10.1016/0012-821X\(70\)90109-3](https://doi.org/10.1016/0012-821X(70)90109-3)
- European Commission, 2019. Communication from the Commission to the European Parliament, the European Council, the Council, the European Economic and Social Committee and the Committee of the Regions.
https://ec.europa.eu/info/sites/info/files/european-green-deal-communication_en.pdf (Accessed 13.05.20).
- Fléhoc, C., Girard, J.-P., Piantone, P., Bodéan, F., 2006. Stable isotope evidence for the atmospheric origin of CO₂ involved in carbonation of MSWI bottom ash. *Appl. Geochem.* 21, 2037–2048. <https://doi.org/10.1016/j.apgeochem.2006.07.011>
- Frías, M., Rodríguez, O., Vigil de la Villa, R., García, R., Martínez-Ramírez, S., Fernandez-Carrasco, L.J., Vegas, I., 2016. The Influence of Activated Coal Mining Wastes on the Mineralogy of Blended Cement Pastes. *J. Am. Ceram. Soc.* 99, 300–307. <https://doi.org/10.1111/jace.13840>
- Fulekar, M.H., Dave, J.M., 2007. Disposal of fly ash—an environmental problem. *Int. J. Environ. Stud.* 26, 191–215. <https://doi.org/10.1080/00207238608710257>
- García, R., Vigil de la Villa, R., Rodríguez, O., Frías, M., 2009. Mineral phases formation on the pozzolan/lime/water system. *Appl. Clay Sci.* 43, 331–335.
<https://doi.org/10.1016/j.clay.2008.09.013>
- García-Lodeiro, I., Fernández-Jiménez, A., Sobrados, I., Sanz, J., Palomo, A., 2012. C-S-H Gels: Interpretation of ²⁹Si MAS-NMR Spectra. *J. Am. Ceram. Soc.* 95, 1440–1446. <https://doi.org/10.1111/j.1551-2916.2012.05091.x>
- Gavrilova, O., Randra, T., Vallner, L., Strandberg, M., Vilu, R., 2005. Life Cycle Analysis of the Estonian Oil Shale Industry. Estonian Fund for Nature, Tallinn University of Technology, Tallinn, pp. 145.
- Gazdič, D., Fridrichová, M., Kulísek, K., Vehovská, L., 2017. The Potential Use of the FBC Ash for the Preparation of Blended Cements. *Procedia Eng., International High-Performance Built Environment Conference – A Sustainable Built Environment Conference 2016 Series (SBE16), iHBE 2016* 180, 1298–1305.
<https://doi.org/10.1016/j.proeng.2017.04.292>
- Geng, A., 2015. Munsell Color Palette. <http://pteromys.melonisland.net/munsell/> (Accessed 28.10.19).
- Golubev, N., 2003. Solid oil shale heat carrier technology for oil shale retorting. *Oil Shale* 20, 324–332.
- Grant, W.D., 2006. Alkaline Environments and Biodiversity, in: Gerday, C., Glansdorff, N. (Eds.), *Extremophiles, Encyclopedia of Life Support Systems (EOLSS)*. Eolss Publishers, Oxford, UK, pp. 20.
- Grossman, E.L., 2012. Applying Oxygen Isotope Paleothermometry in Deep Time. *Paleontol. Soc. Pap.* 18, 39–68. <https://doi.org/10.1017/S1089332600002540>
- Hartshorn, S.A., Sharp, J., Swamy, R.N., 1999. Thauasite formation in Portland-limestone cement pastes. *Cem. Concr. Res.* 29, 1331–1340.
[https://doi.org/10.1016/S0008-8846\(99\)00100-3](https://doi.org/10.1016/S0008-8846(99)00100-3)
- Hays, P.D., Grossman, E.L., 1991. Oxygen isotopes in meteoric calcite cements as indicators of continental paleoclimate. *Geology* 19, 441–444.
[https://doi.org/10.1130/0091-7613\(1991\)019%3C0441:OIIMCC%3E2.3.CO;2](https://doi.org/10.1130/0091-7613(1991)019%3C0441:OIIMCC%3E2.3.CO;2)

- Hyvert, N., Sellier, A., Duprat, F., Rougeau, P., Francisco, P., 2010. Dependency of C–S–H carbonation rate on CO₂ pressure to explain transition from accelerated tests to natural carbonation. *Cem. Concr. Res.* 40, 1582–1589.
<https://doi.org/10.1016/j.cemconres.2010.06.010>
- IPCC, 2007. *Climate Change 2007: Mitigation of Climate Change*. Contribution of Working Group III to the Fourth Assessment Report of the Intergovernmental Panel on Climate Change [B. Metz, O.R. Davidson, P.R. Bosch, R. Dave, L.A. Meyer (eds)], Cambridge University Press, Cambridge, United Kingdom and New York, NY, USA., pp. 851.
- IPCC, 2005. *IPCC Special Report on Carbon Dioxide Capture and Storage*. Prepared by Working Group III of the Intergovernmental Panel on Climate Change [Metz, B., O. Davidson, H. C. de Coninck, M. Loos, and L. A. Meyer (eds.)]. Cambridge University Press, Cambridge, United Kingdom and New York, NY, USA, pp. 442.
- Kann, J., Elenurm, A., Rohtla, I., Golubev, N., Kaidalov, A., Kindorkin, B., 2004. About thermal low-temperature processing of oil shale by solid heat carrier method. *Oil Shale* 21, 195–203.
- Keeling, R.F., Graven, H.D., Welp, L.R., Resplandy, L., Bi, J., Piper, S.C., Sun, Y., Bollenbacher, A., Meijer, H.A.J., 2017. Atmospheric evidence for a global secular increase in carbon isotopic discrimination of land photosynthesis. *Proc. Natl. Acad. Sci.* 114, 10361–10366. <https://doi.org/10.1073/pnas.1619240114>
- Kelemen, P.B., McQueen, N., Wilcox, J., Renforth, P., Dipple, G., Vankeuren, A.P., 2020. Engineered carbon mineralization in ultramafic rocks for CO₂ removal from air: Review and new insights. *Chemical Geology* 550, 119628.
<https://doi.org/10.1016/j.chemgeo.2020.119628>
- Kim, M.S., Jun, Y., Lee, C., Oh, J.E., 2013. Use of CaO as an activator for producing a price-competitive non-cement structural binder using ground granulated blast furnace slag. *Cem. Concr. Res.* 54, 208–214.
<https://doi.org/10.1016/j.cemconres.2013.09.011>
- Konist, A., Maaten, B., Loo, L., Neshumayev, D., Pihu, T., 2016. Mineral sequestration of CO₂ by carbonation of Ca-rich oil shale ash in natural conditions. *Oil Shale* 33, 248–259. <https://doi.org/10.3176/oil.2016.3.04>
- Konist, A., Pihu, T., Neshumayev, D., Siirde, A., 2013. Oil shale pulverized firing: Boiler efficiency, ash balance and flue gas composition. *Oil Shale* 30, 6–18.
<https://doi.org/10.3176/oil.2013.1.02>
- Krishnamurthy, R.V., Schmitt, D., Atekwana, E.A., Baskaran, M., 2003. Isotopic investigations of carbonate growth on concrete structures. *Appl. Geochem.* 18, 435–444.
[https://doi.org/10.1016/S0883-2927\(02\)00089-6](https://doi.org/10.1016/S0883-2927(02)00089-6)
- Kuusik, R., Uibu, M., Kirsimäe, K., Mõtsep, R., Meriste, T., 2012. Open-air deposition of Estonian oil shale ash: Formation, state of art, problems and prospects for the abatement of environmental impact. *Oil Shale* 29, 376–403.
<https://doi.org/10.3176/oil.2012.4.08>
- Kuusik, R., Paat, A., Veskimäe, H., Uibu, M., 2004. Transformations in oil shale ash at wet deposition. *Oil Shale* 21, 27–42.
- Kuusik, R., Uibu, M., Kirsimäe, K., 2005. Characterization of oil shale ashes formed at industrial scale boilers. *Oil Shale* 22, 407–419.
- Kuusik, R., Veskimäe, H., Uibu, M., 2002. Carbon dioxide binding in the heterogeneous systems formed at combustion of oil shale 3. Transformations in the system suspension of ash – Flue gases. *Oil Shale* 19, 277–288.

- Kuusik, R., Veskimäe, H., Kaljuvee, T., Parts, O., 2001. Carbon dioxide binding in the heterogeneous systems formed by combustion of oil shale. 1. Carbon dioxide binding at oil shale ash deposits. *Oil Shale* 18, 109–122.
- Leben, K., Mõtlep, R., Konist, A., Pihu, T., Kirsimäe, K., 2021. Carbon dioxide sequestration in power plant Ca-rich ash waste deposits. *Oil Shale* 38.
- Leben, K., Mõtlep, R., Paaver, P., Konist, A., Pihu, T., Kirsimäe, K., 2020. Geochemical study of stable carbon and oxygen isotopes in landfilled Ca-Rich oil shale ash. *Est. J. Earth Sci.* 69, 134–142. <https://doi.org/10.3176/earth.2020.09>
- Leben, K., Mõtlep, R., Paaver, P., Konist, A., Pihu, T., Paiste, P., Heinmaa, I., Nurk, G., Anthony, E.J., Kirsimäe, K., 2019. Long-term mineral transformation of Ca-rich oil shale ash waste. *Sci. Total Environ.* 658, 1404–1415. <https://doi.org/10.1016/j.scitotenv.2018.12.326>
- Leleu, T., Chavagnac, V., Delacour, A., Noiriel, C., Ceuleneer, G., Aretz, M., Rommevaux, C., Ventalon, S., 2016. Travertines Associated With Hyperalkaline Springs: Evaluation As A Proxy For Paleoenvironmental Conditions And Sequestration of Atmospheric CO₂. *J. Sediment. Res.* 86, 1328–1343. <https://doi.org/10.2110/jsr.2016.79>
- Létolle, R., Gégout, P., Rafai, N., Revertegeat, E., 1992. Stable isotopes of carbon and oxygen for the study of carbonation/decarbonation processes in concretes. *Cem. Concr. Res., Special Double Issue Proceedings of Symposium D of the E-MRS Fall Meeting 1991* 22, 235–240. [https://doi.org/10.1016/0008-8846\(92\)90061-Y](https://doi.org/10.1016/0008-8846(92)90061-Y)
- Lieberman, R.N., Knop, Y., Izquierdo, M., Palmerola, N.M., Rosa, J. de la, Cohen, H., Muñoz-Quirós, C., Cordoba, P., Querol, X., 2018. Potential of hazardous waste encapsulation in concrete with coal fly ash and bivalve shells. *J. Clean. Prod.* 185, 870–881. <https://doi.org/10.1016/j.jclepro.2018.03.079>
- Liira, M., Kirsimäe, K., Kuusik, R., Mõtlep, R., 2009. Transformation of calcareous oil-shale circulating fluidized-bed combustion boiler ashes under wet conditions. *Fuel* 88, 712–718. <https://doi.org/10.1016/j.fuel.2008.08.012>
- Loo, L., Konist, A., Neshumayev, D., Pihu, T., Maaten, B., Siirde, A., 2018. Ash and Flue Gas from Oil Shale Oxy-Fuel Circulating Fluidized Bed Combustion. *Energies* 11, 1218. <https://doi.org/10.3390/en11051218>
- Luukkonen, T., Abdollahnejad, Z., Yliniemi, J., Kinnunen, P., Illikainen, M., 2018. One-part alkali-activated materials: A review. *Cem. Concr. Res.* 103, 21–34. <https://doi.org/10.1016/j.cemconres.2017.10.001>
- L’vov, B.V., 2007. *Thermal Decomposition of Solids and Melts*. Springer, Netherlands, pp. 246. <https://doi.org/10.1007/978-1-4020-5672-7>
- Maaten, B., Loo, L., Konist, A., Pihu, T., Siirde, A., 2017a. Investigation of the evolution of sulphur during the thermal degradation of different oil shales. *J. Anal. Appl. Pyrolysis* 128, 405–411. <https://doi.org/10.1016/j.jaap.2017.09.007>
- Maaten, B., Loo, L., Konist, A., Siirde, A., 2017b. Mineral matter effect on the decomposition of Ca-rich oil shale. *J. Therm. Anal. Calorim.* 131, 2087–2091. <https://doi.org/10.1007/s10973-017-6823-1>
- Macleod, G., Fallick, A.E., Hall, A.J., 1991. The mechanism of carbonate growth on concrete structures, as elucidated by carbon and oxygen isotope analyses. *Chem. Geol. Isot. Geosci. Sect.* 86, 335–343. [https://doi.org/10.1016/0168-9622\(91\)90015-O](https://doi.org/10.1016/0168-9622(91)90015-O)
- Magbitang, R.A., Lamorena, R.B., 2016. Carbonate formation on ophiolitic rocks at different pH, salinity and particle size conditions in CO₂-sparged suspensions. *Int. J. Ind. Chem.* 7, 359–367. <https://doi.org/10.1007/s40090-016-0099-3>

- Magi, M., Lippmaa, E., Samoson, A., Engelhardt, G., Grimmer, A.R., 1984. Solid-state high-resolution silicon-29 chemical shifts in silicates. *J. Phys. Chem.* 88, 1518–1522. <https://doi.org/10.1021/j150652a015>
- Mataalkah, F., Xu, L., Wu, W., Soroushian, P., 2017. Mechanochemical synthesis of one-part alkali aluminosilicate hydraulic cement. *Mater. Struct.* 50. <https://doi.org/10.1617/s11527-016-0968-4>
- McCarthy, M.J., Dhir, R.K., 1999. Towards maximising the use of fly ash as a binder. *Fuel* 78, 121–132. [https://doi.org/10.1016/S0016-2361\(98\)00151-3](https://doi.org/10.1016/S0016-2361(98)00151-3)
- Mickler, P.J., Stern, L.A., Banner, J.L., 2006. Large kinetic isotope effects in modern speleothems. *Geol. Soc. Am. Bull.* 118, 65–81. <https://doi.org/10.1130/B25698.1>
- Montes-Hernandez, G., Pérez-López, R., Renard, F., Nieto, J.M., Charlet, L., 2009. Mineral sequestration of CO₂ by aqueous carbonation of coal combustion fly-ash. *J. Hazard. Mater.* 161, 1347–1354. <https://doi.org/10.1016/j.jhazmat.2008.04.104>
- Mõtlep, R., Sild, T., Puura, E., Kirsimäe, K., 2010. Composition, diagenetic transformation and alkalinity potential of oil shale ash sediments. *J. Hazard. Mater.* 184, 567–573. <https://doi.org/10.1016/j.jhazmat.2010.08.073>
- Myers, R.J., Bernal, S.A., San Nicolas, R., Provis, J.L., 2013. Generalized Structural Description of Calcium–Sodium Aluminosilicate Hydrate Gels: The Cross-Linked Substituted Tobermorite Model. *Langmuir* 29, 5294–5306. <https://doi.org/10.1021/la4000473>
- Myers, R.J., L'Hôpital, E., Provis, J.L., Lothenbach, B., 2015. Effect of temperature and aluminium on calcium (alumino)silicate hydrate chemistry under equilibrium conditions. *Cem. Concr. Res.* 68, 83–93. <https://doi.org/10.1016/j.cemconres.2014.10.015>
- Nationally Determined Contribution to the Paris Agreement Update of the NDC of the European Union and its Member States https://www4.unfccc.int/sites/ndcstaging/PublishedDocuments/Estonia%20First/EU_NDC_Submission_December%202020.pdf (Accessed 29.12.2020).
- Neshumayev, D., Pihu, T., Siirde, A., Järvik, O., Konist, A., 2019. Solid heat carrier oil shale retorting technology with integrated CFB technology. *Oil Shale* 36, 99–113. <https://doi.org/10.3176/oil.2019.2S.02>
- Nguyen, L.C., Inui, T., Ikeda, K., Katsumi, T., 2015. Aging effects on the mechanical property of waste mixture in coastal landfill sites. *Soils Found.* 55, 1441–1453. <https://doi.org/10.1016/j.sandf.2015.10.009>
- Nishikawa, T., Suzuki, K., Ito, S., Sato, K., Takebe, T., 1992. Decomposition of synthesized ettringite by carbonation. *Cem. Concr. Res.* 22, 6–14. [https://doi.org/10.1016/0008-8846\(92\)90130-N](https://doi.org/10.1016/0008-8846(92)90130-N)
- O'Connor, W., Dahlin, D.C., Rush, G.E., Gerdemann, S.J., Penner, L.R., Nilsen, D.N., 2005. Aqueous Mineral Carbonation: Mineral Availability, Pretreatment, Reaction Parametrics, and Process Studies. DOE/ARC-TR-04-002, Albany Research Center, Albany, New York, pp. 463. <https://doi.org/10.13140/RG.2.2.23658.31684>
- Ochedi, F.O., Liu, Y., Adewuyi, Y.G., 2020. State-of-the-art review on capture of CO₂ using adsorbents prepared from waste materials. *Process Safety and Environmental Protection* 139, 1–25. <https://doi.org/10.1016/j.psep.2020.03.036>
- Olajire, A.A., 2013. A review of mineral carbonation technology in sequestration of CO₂. *J. Pet. Sci. Eng.* 109, 364–392. <https://doi.org/10.1016/j.petrol.2013.03.013>
- Oskierski, H.C., Dlugogorski, B.Z., Jacobsen, G., 2013. Sequestration of atmospheric CO₂ in chrysotile mine tailings of the Woodsreef Asbestos Mine, Australia:

- Quantitative mineralogy, isotopic fingerprinting and carbonation rates. *Chem. Geol.* 358, 156–169. <https://doi.org/10.1016/j.chemgeo.2013.09.001>
- Ots, A., 2006. Oil shale fuel combustion. Tallinna Raamatutrükikoda, Tallinn, pp. 833.
- Paaver, P., Paiste, P., Mõtlep, R., Kirsimäe, K., 2017. Self-cementing properties and alkali activation of enefit280 solid heat carrier retorting ash. *Oil Shale* 34, 263–278. <https://doi.org/10.3176/oil.2017.3.05>
- Paiste, P., Külaviir, M., Paaver, P., Heinmaa, I., Vahur, S., Kirsimäe, K., 2017. Beneficiation of Oil Shale Processing Waste: Secondary Binder Phases in Alkali Activated Composites. *Waste Biomass Valorization* 10, 1407–1417. <https://doi.org/10.1007/s12649-017-0140-6>
- Pan, S.Y., Chang, E.E., Chiang, P.C., 2012. CO₂ capture by accelerated carbonation of alkaline wastes: A review on its principles and applications. *Aerosol Air Qual. Res.* 12, 770–791. <https://doi.org/10.4209/aaqr.2012.06.0149>
- Pihu, T., Arro, H., Prikk, A., Rootamm, R., Konist, A., Kirsimäe, K., Liira, M., Mõtlep, R., 2012. Oil shale CFBC ash cementation properties in ash fields. *Fuel* 93, 172–180. <https://doi.org/10.1016/j.fuel.2011.08.050>
- Pihu, T., Konist, A., Puura, E., Liira, M., Kirsimäe, K., 2019. Properties and environmental impact of oil shale ash landfills. *Oil Shale* 36, 257–270. <https://doi.org/10.3176/oil.2019.2.01>
- Pronost, J., Beaudoin, G., Tremblay, J., Larachi, F., Duchesne, J., Hébert, R., Constantin, M., 2011. Carbon Sequestration Kinetic and Storage Capacity of Ultramafic Mining Waste. *Environ. Sci. Technol.* 45, 9413–9420. <https://doi.org/10.1021/es203063a>
- Punning, J.-M., Toots, M., Vaikmäe, R., 1987. Oxygen-18 in Estonian Natural Waters. *Isotopenpraxis Isotopes in Environmental and Health Studies* 23, 232–234. <https://doi.org/10.1080/10256018708623797>
- Raado, L.-M., Kuusik, R., Hain, T., Uibu, M., Somelar, P., 2014. Oil shale ash based stone formation – Hydration, hardening dynamics and phase transformations. *Oil Shale* 31, 91–101. <https://doi.org/10.3176/oil.2014.1.09>
- Rattanasak, U., Chindaprasirt, P., 2009. Influence of NaOH solution on the synthesis of fly ash geopolymer. *Miner. Eng.* 22, 1073–1078. <https://doi.org/10.1016/j.mineng.2009.03.022>
- Richardson, I.G., 2004. Tobermorite/jennite- and tobermorite/calcium hydroxide-based models for the structure of C-S-H: applicability to hardened pastes of tricalcium silicate, β -dicalcium silicate, Portland cement, and blends of Portland cement with blast-furnace slag, metakaolin, or silica fume. *Cem. Concr. Res.* 34, 1733–1777. <https://doi.org/10.1016/j.cemconres.2004.05.034>
- Richardson, I.G., 1999. The nature of C-S-H in hardened cements. *Cem. Concr. Res.* 29, 1131–1147. [https://doi.org/dx.doi.org/10.1016/S0008-8846\(99\)00168-4](https://doi.org/dx.doi.org/10.1016/S0008-8846(99)00168-4)
- Richardson, I.G., Cabrera, J.G., 2000. The nature of C-S-H in model slag-cements. *Cem. Concr. Compos.* 22, 259–266. [https://doi.org/10.1016/S0958-9465\(00\)00022-6](https://doi.org/10.1016/S0958-9465(00)00022-6)
- Sanna, A., Uibu, M., Caramanna, G., Kuusik, R., Maroto-Valer, M.M., 2014. A review of mineral carbonation technologies to sequester CO₂. *Chem. Soc. Rev.* 43, 8049–8080. <https://doi.org/10.1039/C4CS00035H>
- Scrivener, K., Snellings, R., Lothenbach, B., 2016. A Practical Guide to Microstructural Analysis of Cementitious Materials. CRC Press, pp.509.
- Sear, L., 2006. Pulverised Fuel Ash and Preventing the Thaumassite Form of Sulfate Attack, in: *AshTech 2006: Proceedings of the International Conference*. Presented at

- the Ash Technology Conference 2006, UKQAA, Hippodrome Theatre, Birmingham, United Kingdom.
- Sedman, A., Talviste, P., Kirsimäe, K., 2012. The study of hydration and carbonation reactions and corresponding changes in the physical properties of co-deposited oil shale ash and semicoke wastes in a small-scale field experiment. *Oil Shale* 29, 279–294. <https://doi.org/10.3176/oil.2012.3.07>
- Stansell, N.D., Klein, E.S., Finkenbinder, M.S., Fortney, C.S., Dodd, J.P., Terasmaa, J., Nelson, D.B., 2017. A stable isotope record of Holocene precipitation dynamics in the Baltic region from Lake Nuudsaku, Estonia. *Quat. Sci. Rev.* 175, 73–84. <https://doi.org/10.1016/j.quascirev.2017.09.013>
- Statistics Estonia, 2016. Statistical Yearbook of Estonia 2016 (Pöder, K, ed.). Tallinn, pp. 441.
- Stutzman, P.E., 2001. Scanning electron microscopy in concrete petrography. *Natl. Inst. Stand. Technol.* 2, 59–72.
- Suzuki, K., Nishikawa, T., Ito, S., 1985. Formation and carbonation of C-S-H in water. *Cem. Concr. Res.* 15, 213–224. [https://doi.org/10.1016/0008-8846\(85\)90032-8](https://doi.org/10.1016/0008-8846(85)90032-8)
- Swart, P.K., 2015. The geochemistry of carbonate diagenesis: The past, present and future. *Sedimentology* 62, 1233–1304. <https://doi.org/10.1111/sed.12205>
- Talviste, P., Sedman, A., Mõtlep, R., Kirsimäe, K., 2013. Self-cementing properties of oil shale solid heat carrier retorting residue. *Waste Manag. Res.* 31, 641–647. <https://doi.org/10.1177/0734242X13482033>
- Taylor, H.F.W., 1997. Cement chemistry, 2nd ed. T. Telford, London, pp. 459.
- Teboul, P.-A., Durllet, C., Gaucher, E.C., Virgone, A., Girard, J.-P., Curie, J., Lopez, B., Camoin, G.F., 2016. Origins of elements building travertine and tufa: New perspectives provided by isotopic and geochemical tracers. *Sediment. Geol.* 334, 97–114. <https://doi.org/10.1016/j.sedgeo.2016.01.004>
- Torres, S.M., Kirk, C.A., Lynsdale, C.J., Swamy, R.N., Sharp, J.H., 2004. Thaumasite-ettringite solid solutions in degraded mortars. *Cem. Concr. Res.* 34, 1297–1305. <https://doi.org/10.1016/j.cemconres.2003.09.016>
- Trikkel, A., Keelmann, M., Kaljuvee, T., Kuusik, R., 2010. CO₂ and SO₂ uptake by oil shale ashes: Effect of pre-treatment on kinetics. *J. Therm. Anal. Calorim.* 99, 763–769. <https://doi.org/10.1007/s10973-009-0423-7>
- Turvey, C.C., Wilson, S.A., Hamilton, J.L., Tait, A.W., McCutcheon, J., Beinlich, A., Fallon, S.J., Dipple, G.M., Southam, G., 2018. Hydrotalcites and hydrated Mg-carbonates as carbon sinks in serpentinite mineral wastes from the Woodsreef chrysotile mine, New South Wales, Australia: Controls on carbonate mineralogy and efficiency of CO₂ air capture in mine tailings. *Int. J. Greenh. Gas Control* 79, 38–60. <https://doi.org/10.1016/j.ijggc.2018.09.015>
- Uibu, M., Kuusik, R., 2014. Main physicochemical factors affecting the aqueous carbonation of oil shale ash. *Miner. Eng., Accelerated Carbonation for Environmental and Materials Engineering* 59, 64–70. <https://doi.org/10.1016/j.mineng.2013.10.013>
- Uibu, M., Kuusik, R., Veskimäe, H., 2008. Seasonal binding of atmospheric CO₂ by oil shale ash. *Oil Shale* 25, 254–266. <https://doi.org/10.3176/oil.2008.2.07>
- Uibu, M., Somelar, P., Raado, L.-M., Irha, N., Hain, T., Koroljova, A., Kuusik, R., 2016. Oil shale ash based backfilling concrete – Strength development, mineral transformations and leachability. *Constr. Build. Mater.* 102, 620–630. <https://doi.org/10.1016/j.conbuildmat.2015.10.197>
- Uibu, M., Uus, M., Kuusik, R., 2009. CO₂ mineral sequestration in oil-shale wastes from Estonian power production. *J. Environ. Manage.* 90, 1253–1260.

- Uibu, M., Velts, O., Kuusik, R., 2010. Developments in CO₂ mineral carbonation of oil shale ash. *J. Hazard. Mater.* 174, 209–214.
- Ukrainczyk, N., Ukrainczyk, M., Šipušić, J., Matusinović, T., 2006. XRD and TGA Investigation of Hardened Cement Paste Degradation. 11 Int. Conf. Mater. Process. Frict. Wear MATRIB06 243–249.
- Velts, O., Uibu, M., Kallas, J., Kuusik, R., 2013. CO₂ Mineralisation: Concept for Co-utilization of Oil Shale Energetics Waste Streams in CaCO₃ Production. *Energy Procedia*, GHGT-11 Proceedings of the 11th International Conference on Greenhouse Gas Control Technologies, 18–22 November 2012, Kyoto, Japan 37, 5921–5928. <https://doi.org/10.1016/j.egypro.2013.06.518>
- Velts, O., Uibu, M., Kallas, J., Kuusik, R., 2011. CO₂ mineral trapping: Modeling of calcium carbonate precipitation in a semi-batch reactor. *Energy Procedia* 4, 771–778. <https://doi.org/10.1016/j.egypro.2011.01.118>
- Whiticar, M.J., 1999. Carbon and hydrogen isotope systematics of bacterial formation and oxidation of methane. *Chem. Geol.* 161, 291–314. [https://doi.org/10.1016/S0009-2541\(99\)00092-3](https://doi.org/10.1016/S0009-2541(99)00092-3)
- Wilson, S.A., Harrison, A.L., Dipple, G.M., Power, I.M., Barker, S.L.L., Ulrich Mayer, K., Fallon, S.J., Raudsepp, M., Southam, G., 2014. Offsetting of CO₂ emissions by air capture in mine tailings at the Mount Keith Nickel Mine, Western Australia: Rates, controls and prospects for carbon neutral mining. *Int. J. Greenh. Gas Control* 25, 121–140. <https://doi.org/10.1016/j.ijggc.2014.04.002>
- Wu, B., Ye, G., 2016. Carbonation mechanism of different kinds of C-S-H: rate and products, in: *Proceedings of the International RILEM Conference Materials, Systems and Structures in Civil Engineering 2016, Segment on Concrete with Supplementary Cementitious Materials*, 22–24 August 2016, (Jensen, O. M., Kovler, K., De Belie, N., Eds.). Presented at the RILEM 2016, Technical University of Denmark, Lyngby, Denmark, pp. 263–272.
- Yadav, S., Mehra, A., 2021. A review on ex situ mineral carbonation. *Environ. Sci. Pollut. Res.* <https://doi.org/10.1007/s11356-020-12049-4>
- Yamasaki, A., 2003. An Overview of CO₂ Mitigation Options for Global Warming—Emphasizing CO₂ Sequestration Options. *J. Chem. Eng. Jpn.* 36, 361–375. <https://doi.org/10.1252/jcej.36.361>
- Yip, C.K., Lukey, G.C., van Deventer, J.S.J., 2005. The coexistence of geopolymeric gel and calcium silicate hydrate at the early stage of alkaline activation. *Cem. Concr. Res.* 35, 1688–1697. <https://doi.org/10.1016/j.cemconres.2004.10.042>
- Yu, P., Kirkpatrick, R.J., Poe, B., McMillan, P., Cong, X., 1999. Structure of Calcium Silicate Hydrate (C-S-H): Near-, Mid-, and Far-Infrared Spectroscopy. *J. Am. Ceram. Soc.* 82, 742–748. <https://doi.org/10.1111/j.1151-2916.1999.tb01826.x>
- Yvon, J., Antenucci, D., Jdid, E.-A., Lorenzi, G., Dutre, V., Leclercq, D., Nielsen, P., Veschkens, M., 2006. Long-term stability in landfills of Municipal Solid Waste Incineration fly ashes solidified/stabilized by hydraulic binders. *J. Geochem. Explor.* 90, 143–155. <https://doi.org/10.1016/j.gexplo.2005.09.008>
- Yörük, C.R., Uibu, M., Usta, M.C., Kaljuvee, T., Trikkel, A., 2020. CO₂ mineralization by burnt oil shale and cement bypass dust: effect of operating temperature and pre-treatment. *J. Therm. Anal. Calorim.* 142, 991–999. <https://doi.org/10.1007/s10973-020-09349-9>
- Zhang, Z., Pan, S.-Y., Li, H., Cai, J., Olabi, A.G., Anthony, E.J., Manovic, V., 2020. Recent advances in carbon dioxide utilization. *Renewable and Sustainable Energy Reviews* 125, 109799. <https://doi.org/10.1016/j.rser.2020.109799>

- Zhang, Q., Ye, G., 2012. Dehydration kinetics of Portland cement paste at high temperature. *J. Therm. Anal. Calorim.* 110, 153–158.
<https://doi.org/10.1007/s10973-012-2303-9>
- Zhao, S., Duan, Y., Lu, Jincheng, Gupta, R., Pudasainee, D., Liu, S., Liu, M., Lu, Jianhong, 2018. Chemical speciation and leaching characteristics of hazardous trace elements in coal and fly ash from coal-fired power plants. *Fuel* 232, 463–469.
<https://doi.org/10.1016/j.fuel.2018.05.135>
- Zhou, Q., Hill, J., Byars, E.A., Cripps, J.C., Lynsdale, C.J., Sharp, J.H., 2006. The role of pH in thaumasite sulfate attack. *Cem. Concr. Res.* 36, 160–170.
<https://doi.org/10.1016/j.cemconres.2005.01.003>

SUMMARY IN ESTONIAN

Eesti kaltsiumirikka põlevkivituhasette pikaajaline diagenees ja CO₂ sidumisvõime

Fossiilseid tahkeid kütuseid kasutav energeetikasektor põhjustab nii suure osa globaalsete kasvuhoonegaaside emissioonidest kui ka suures koguses erinevaid tahkeid jäätmeid. Selliste fossiilsete kütuste nagu kivisüsi ja põlevkivi põletamisel tekkivad tahked jäätmed on tihti keemiliselt reaktiivsed. Et selliste jäätmete taaskasutus on piiratud, ladestatakse need elektrijaamade lähedal paiknevatesse settetiikidesse või -platodele. Avatud tingimustes ladustatud jäätmete potentsiaalne keskkonnamõju sõltub jäätmete keemilis-mineraalsest koostisest, põletus- ja utmisprotsesside tehnoloogiast, jäätmekäitlusmeetoditest ning kliimatilistest tingimustest (Fulekar ja Dave, 2007). Teisalt on paljudel tahketel põletusjäätmetel mitmeid taaskasutusvõimalusi, näiteks on neid võimalik kasutada lisandina betooni ja ehitusmaterjalide tootmisel või kaevandatud alade tagasitäitmisel. Taaskasutuse maht aga varieerub palju: Eestis on see vaid mõni protsent, aga Jaapanis ligikaudu 90% (Bobicki et al., 2012; Lieberman et al., 2018; McCarthy ja Dhir, 1999).

Pikaajalise kliimapolitiika eesmärkide saavutamiseks (nt Pariisi kliimakokkulepe) on mõeldavamat, et fossiilkütuste kasutamist hakatakse järkjärguliselt tulevate aastakümnetel vähendada. Juba 2050. aastaks on Euroopa Liidus eesmärgiks seatud süsinikuneutraalne majandus (European Commission, 2019), mille saavutamiseks tuleb kasutada erinevaid CO₂ heitmeid vähendavaid meetmeid, sealhulgas juba õhku paisatud CO₂ heitmete vähendamise tehnoloogiad sh geoloogilise sidumise ja ladustamise meetodid (Aminu et al., 2017; Bui et al., 2018; IPCC, 2007, 2005; Sanna et al., 2014; Yamasaki, 2003). Tehnoloogia valmidusastme poolest on neist kohe rakendatav CO₂ geoloogiline ladustamine maa-alustes struktuurides, samuti ka selle lahustamine kõrge soolsusega põhjaveekihtides ning adsorbeerimine erinevates orgaanikarikastes kivimites nagu kivisüsi või põlevkivi. Ladustamiseks kasutatavad geoloogilised formatsioonid peavad tagama CO₂ pikaajalise sidustumise ja peaksid võimalike lekete ohu minimeerimiseks täitma rangeid tingimusi. CO₂ maa-alust ladustamist on kasutatud juba aastakümneid naftamaardlates naftasaagise tõstmiseks. Selline praktika ei aita aga kaasa süsinikuheite mahtude vähenemisele, kuna lisanduv nafta ja selle kasutamine kütusena nullib ladustatava CO₂ mõju süsinikutasakaalule.

Teine laialdaselt uuritav süsiniku sidumise ja ladustamise meetod on CO₂ sidumine stabiilsetes karbonaatsetes mineraalides. Põhimõtteliselt toimib see meetod sarnaselt looduslike silikaatsete mineraalide murenemisega, kus vabanevad Ca(Mg) seovad stabiilsesse Ca- või Mg karbonaadi vormi atmosfääre CO₂. Lisaks looduslike leelismuldmetallide oksiidide (CaO ja MgO) sisaldavate mineraalide/kivimite, nagu näiteks ultraaluselised tardkivimid, saab potentsiaalse reaktiivse lähtematerjalina kasutada nii erinevaid aluselisi kaevandusjäätmeid (Oskierski et al., 2013; Pronost et al., 2011; Wilson et al., 2014), kui ka selliseid

energiatööstuse jäätmeid nagu kivilöö- või põlevkivituhka, terasetööstuse šlakki jne (Bobicki et al., 2012; Olajire, 2013; Pan et al., 2012; Sanna et al., 2014).

Süsiniku mineraalset karboniseerumist on võimalik läbi viia sobivate looduslike geoloogiliste tingimustega asukohtades *in-situ* või jäätmehooldlates, kui ka *ex-situ* CO₂ lähteallikate juures enne materjali lõplikku ladustamist. Selliseks CO₂ ladustamiseks sobivad erinevad kõrge CaO ja MgO sisaldusega tööstusjäätmed, millel on kõrge reaktiivsus ja kõrge süsiniku sidumise potentsiaal. Näiteks on vaid 4,1% CaO sisaldusega kivilööetuhk võimeline ühe tonni kohta siduma kuni 26 kg süsinikdioksiidi (Montes-Hernandez et al., 2009). Erinevalt kivilööetuhast on vaba CaO sisaldus Eesti põlevkivituhkades kuni 30%, kuid sellest ei piisa kaugeltki põlevkivitööstuse poolt õhku paisatud CO₂ tagasisidumiseks (Konist et al. (2016) hinnangul potentsiaalselt võimalik siduda vaid ca 5–6% põletamisel emiteeritud CO₂-st). Küll aga on juba tekkinud ja ladestatud põlevkivituhhal pikaajaline perspektiiv CO₂ tagasisidumiseks ja tekitatud kahju leevendamiseks.

Eesti põlevkivi ehk kukersiit kuulub kerogeensete fossiilsete kütuste hulka ning kuigi põlevkivilasundid on levinud üle terve maailma, siis tööstuslikku kasutust leiavad need tüüpiliselt suhteliselt madala orgaanilise ainese sisaldusega kütused vaid mõnes üksikus riigis. Eestis tööstuslikult kasutatav kukersiit on üks kõrgeima orgaanikasisaldusega põlevkividest, mille kütteväärtust varieerub 8–12 MJ/kg (Ots, 2006) ning mille tuhasus on 45–53% (Konist et al., 2016; Loo et al., 2018; Maaten et al., 2017b, 2017a). Võrdlusena on kivilöö kütteväärtus tavaliselt 26–33 MJ/kg ja tuhasus 5–20%.

Eesti energiasektor on palju aastakümneid sõltunud põlevkivitööstusest. Ühelt poolt on põlevkivi kasutamine alates 1960ndatest kuni viimaste aastateni taganud Eesti energeetilise julgeoleku. Teisalt on põlevkivitööstus aga ka riigi suurim kasvuhoonegaaside emiteerija ja tahkete jäätmete tekitaja, olles ajalooliselt tekitanud üle 70% Eestis emiteeritud CO₂-st (Statistics Estonia, 2016). Euroopa Liidu andmetel oli Eesti 2018. aastal ühe inimese kohta 18,6 tonniga suurim CO₂ emiteerija Euroopas (Crippa et al., 2019). Siiski, alates 2019. aastast on põlevkivitööstuse poolt emiteeritud CO₂ kogused vähenenud ligi poole võrra (Eesti Energia, 2019). Selle peamiseks põhjuseks on süsinikuemissiooni kvootide hinna tõus Euroopa Liidu heitkogustega kauplemise süsteemis (EU ETS), mille tulemusena on Eesti põlevkivienergia muutunud Nord Pooli energiaturul vähem konkurentsivõimeliseks (Elering, 2014).

Langusele vaatamata on viimastel aastatel Eestis kaevandatud igal aastal ligikaudu 15 miljonit tonni põlevkivi (kadusid arvestamata oli mahuks 2019. aastal 12,1 miljonit tonni) ning selle töötlemise tulemusena tekkis igal aastal 6–8 miljonit tonni kaltsiumirikast tuhka. Tekkinud tuhast leiab taaskasutust vaid kuni paar protsenti, põhiliselt lisandina tsemenditööstuses ning mullaparendajana põllumajanduses. Valdav osa tuhast aga ladustatakse koos veega elektri jaamade lähedal tuhaväljadel (Konist et al., 2016; Mõtlep et al., 2010).

Kuna Ca-rikas tuhk (vaba CaO sisaldus ulatub kuni ca 30%-ni; Pihu et al., 2019) on kõrge reaktiivsusega, algab veega kokkupuutel tuha hüdraatumine. Selle tulemusena moodustuvad erinevad sekundaarsed Ca-mineraalid nagu

Ca-hüdroksiid ehk portlandiit, ettringiit, hüdrokalumiit ja paljud teised, mis parandavad tuhasette tsementeerumisomadusi ning võimaldavad ehitada mitmekümne meetri kõrguseid järskude nõlvadega tuhahoidlaid. Paraku on põlevkivituha hüdraatumisel moodustuvad sekundaarsed Ca-faasid avatud keskkonningimustel metastabiilsed ning aja jooksul need kas lagunevad või kristalliseeruvad ümber uuteks diagenetilisteks faasideks. Hüdraatunud kaltsiumirikka põlevkivituha diageneesi ning tsementeerumist on põhjalikult iseloomustatud varasemates laboriuuringutes (Liira et al., 2009; Velts et al., 2013; Raado et al., 2014; Uibu et al., 2016), kuid tuhamägedes toimuvad looduslikes tingimustes pikaajalised muutused ning karboniseerumise reaktsioonide ulatus on sisuliselt teadmata. Ka mujal maailmas läbi viidud tuhaladestute *in-situ* mineraloogilise ja mehaanilise stabiilsuse eksperimentaalsed uuringud on üldjuhul keskendunud mõne aasta jooksul toimuvatele lühiajalistele muutustele (Yvon et al., 2006; Nguyen et al., 2015). Puuduvad uuringud, mis selgitaks metastabiilsete tuhasetete käitumist aastakümneid vältavates diagenetilistes protsessides. Mõtsep et al. (2010) tulemused viitavad, et erinevalt laboritingimustest on tuhasette lasundis karboniseerumine piiratud ning täielik neutraliseerumine võtaks aeglase CO₂ transpordi tõttu tõenäoliselt aega sadu tuhandeid aastaid.

Käesolev doktoritöö uurib Eesti suurimate elektrijaamade juures ladustatud kaltsiumirikka põlevkivituha diagenetilisi muutusi, mis on toimunud enam kui 50 aasta vältel, ning juba ladestatud tuhasette CO₂ sidumise potentsiaali. Uuringu peamisteks eesmärkideks oli:

- selgitada Ca-rikaste tuhajäätmete diagenetilise transformeerumise protsesse ja moodustunud faasid ning hinnata tuhaladestute pikaajalist mehaanilist stabiilsust;
- selgitada tuhaplatoode loodusliku karboniseerumise ulatus ja seda kontrolliva CO₂ allikad;
- selgitada Ca-rikaste põlevkivituhaladestute pikaajalise CO₂ reaalne sidumisvõime ja selle jääkpotentsiaal.

Doktoritöö keskne hüpotees väidab, et Ca-rikka põlevkivituha kiirel ladestamisel ja esmasel karboniseerumisel piiratakse sette kokkupuude atmosfäärse süsinikdioksiidiga ja tuhaladestuses püsib kõrge leeliselisus (pH>10–12). Nendes tingimustes toimub silikaatsete mineraalide ja (pool-)amorfsete klaasjate faaside looduslik leelisaktivatsioon, mis võib suurendada ladestatud materjali mehaanilist stabiilsust, kuid vähendab selle CO₂ sidumise lühiajalist potentsiaali.

Doktoritöö näitab, et looduslikult kõrge leeliselisusega tuhahoidlas moodustuvad tuhasette leelisaktivatsiooni tulemusena sekundaarsed röntgenamorfseid polümeersed kaltsium-(alumiinium)-silikaat-hüdraat ehk C-(A)-S-H faasid. C-S-H geeljad faasid moodustuvad erinevate primaarsete mineraalide ning klaasjate amorfsete faaside aeglasel lahustumisel ning ümberkristalliseerumisel. Eesti Elektriamaa 1960ndate aastate lõpust alates moodustatud tuhahoidla läbilõikes kasvab selliste faaside sisaldus ligikaudu 25%-lt settelasundi pinnakihtides rohkem kui 60%-ni alumistes kihtides. Tuhasete tuumamagnetresonants spektroskoopia (29Si NMR) uuring näitas, et moodustunud C-S-H faaside

struktuuri keerukus ja polümeeriahelate pikkus kasvab koos settekihi vanusega noorematest pinnakihtidest vanemate põhjakihtide suunas. See näitab, et tuhahoidlate diagenetilised muutused toimuvad kõrgelt aluselistes tingimustes aastakümnete jooksul edasi. Nendes protsessides moodustuvad C-S-H ja arvata-vasti ka keerukamad C-A-S-H tüüpi faasid aitavad aja jooksul parandada tuhasette mehaanilist tugevust ja seeläbi tuhahoidlate pikaajalist püsivust.

Samas esinevad Eesti Elektri jaama tuhahoidla setetes tasemed, kus ilmneb osaline C-S-H faaside lahustumine ning nn hilise ettringiidi-thaumasiidi moodustumine. See puudutab ennekõike poorsemaid, kõrgema vee juhtivusega kihte. Et thaumasiit on ebastabiilne faas, võib selliste tsoonide kujunemine vähendada aja jooksul settematerjali mehaanilist tugevust ja suurendada nõlvade varisemise ohtu.

Tuhasettes moodustunud sekundaarseid karbonaatseid faase iseloomustavad negatiivsed $\delta^{13}\text{C}$ ja $\delta^{18}\text{O}$ stabiilsete isotoopide väärtused. $\delta^{13}\text{C}$ CV-PDB väärtused varieeruvad $-12\text{-st } -24\text{‰}$ -ni ning $\delta^{18}\text{O}$ OV-PDB väärtused $-8\text{-st } -15\text{‰}$ -ni. Kuigi ^{13}C suhtes sedavõrd vaesunud süsiniku isotoopkoostis võiks viidata orgaanilist päritolu süsiniku (CO_2) allikale, siis arvatavasti on tegemist leeliselise keskkonna ja piiratud süsihappegaasi difusiooni tulemusel toimuvate mittetasakaaluliste kineetilistelt kontrollitud isotoopse fraktsioneerumise protsessidega. Aluselistes tingimustes on karboniseerumisel toimival süsinikdioksiidi difusioonil läbi portlandiiti ümbritseva veekile eelistatud kergema ^{12}C isotoobiga CO_2 , mis põhjustab tekkiva karbonaadi C-isotoopkoostise tuntava vaesumise raskema C-isotoobi suhtes. Mittetasakaalulised fraktsioneerumisprotsessid põhjustavad samuti ^{18}O suhtes vaesunud karbonaatide isotoopkoostise kujunemise.

Tuhahoidlatesse ladustatud materjali CO_2 sidumise potentsiaali uuring näitab, et tuhasette mineraalne koostis on suure varieeruvusega. CO_2 on tuhasette mineraalides seotud valdavalt karbonaatide koostises ning keskmine CO_2 sisaldus kõigub uuritud läbilõigetel $1,6\text{--}8,9\text{ ‰}$ -ni. Arvestades karbonaatidega seotud CO_2 -le lisaks ka sekundaarses Ca-silikaadis thaumasiidis seotava süsinikdioksiidi osakaalu (ligikaudu 6% koguhulgast), on Eesti tuhaplatoodes mineraalselt seotud ühe tonni tuhasette kohta keskmiselt 51 kg CO_2 -te. See näitaja on varasemate mudelite ja laborieksperimentidel põhinevate CO_2 sidumise hinnangutest vähemalt $5\text{--}6$ korda väiksem. Tolmpõletuskateldel pärit põlevkivituha CO_2 tagasi-sidumise potentsiaali on teoreetiliste arvutuste kaudu hinnatud $350\text{--}500$ kilogrammiks ühe tonni kohta, millest $30\text{--}50\%$ moodustab vaba lubja (hüdraatunult portlandiidi) poolt seotav CO_2 (Uibu ja Kuusik, 2014).

Ladestatud tuhasette piiratud karboniseerumise põhjuseks on tuhamaterjali kiire mattumine ning välimiste settekihtide tsementeerumine, mistõttu jõuab karboniseeruda vaid tuhaplatoo välisperimeeter. Kuigi viimastel aastatel esinenud põlevkivielekttri tootmise ja ladustatava tuha mahtude langustrend toob tänu tuhasette pinnakihtide pikemale kontaktile atmosfääriga tõenäoliselt kaasa ka kõrgema süsinikdioksiidi sidumise määra, siis platoo sisemuses oodatud CO_2 sidumise potentsiaali lähiperspektiivis ei saavutata.

Tuhasette CO₂ sidumise potentsiaali on võimalik tõsta, kui rakendada aktiivset *in-situ* karboniseerumist, kasutades selleks lähedalasuvate elektrijaamade või teiste tööstuste suitsugaase või CO₂ heitmeid, juhtides need läbi tuhahoidlate. Arvestades, et tuhasette koostise peamised mineraalsed faasid, nagu portlandiit, ettringiit ja C-S-H, karboniseeruvad täielikult, on võimalik tõsta tuhka seotud CO₂ mahtu keskmiselt 150 kg võrra tonni kohta, mis tõstaks tuhasette keskmise potentsiaalse süsiniku sidumise mahu hinnanguliselt 200 kg-ni ühe tonni tuhasette kohta.

ACKNOWLEDGEMENTS

I am very grateful to my supervisor Riho Mõtlep for his help during my PhD studies. I recognize all my co-authors for their contributions to my work as well as all colleagues and workers at the Department of Geology for their help during various parts of my work. Mari Aigro is acknowledged for language corrections. Special thanks go to all the past and present occupants of Room 3005. Financial support from the Doctoral School of Earth Sciences and Ecology and the Archimedes Foundation are acknowledged. Finally, I would like to thank my family and friends for their support through the years.

PUBLICATIONS

CURRICULUM VITAE

Name: Kristjan Leben
Date of birth: 17.10.1989
Address: Department of Geology, University of Tartu,
Ravila 14A, 50411 Tartu, Estonia
Contact: Tel. +372 58176460
E-mail: kristjan.leben@ut.ee

Education

2016–... University of Tartu, Department of Geology, PhD student in geology
2012–2015 University of Tartu, MSc in geotechnology
2009–2012 University of Tartu, BSc in environmental technology

Professional employment

2021–... Analyst, University of Tartu, Department of Geology
2017–2020 Junior Research Fellow of Geology, University of Tartu, Department of Geology
2014 Specialist in Geology, University of Tartu, Department of Geology

Field of research:

Environmental technology, geochemistry, minearology,

Publications

1. **Leben, K.**; Mötlep, R.; Paaver, P.; Konist A.; Pihu, T.; Paiste, P.; Heinmaa, I.; Nurk, G.; Anthony, E.; Kirsimäe, K. (2019). Long-term mineral transformation of Ca-rich oil shale ash waste. *Science of the Total Environment* 658, 1404–1415.
2. **Leben, K.**; Mötlep, R.; Paaver, P.; Konist A.; Pihu, T.; Kirsimäe, K. (2020). Geochemical study of stable carbon and oxygen isotopes in landfilled Ca-rich oil shale ash. *Estonian Journal of Earth Sciences* 69 (3), 134–142.
3. **Leben, K.**; Mötlep, R.; Konist A.; Pihu, T.; Kirsimäe, K. (2021). Carbon dioxide sequestration in power plant Ca-rich ash waste deposits. *Oil Shale* 38 (1), 65–88.

ELULOOKIRJELDUS

Nimi: Kristjan Leben
Sünniaeg: 17.10.1989
Aadress: Geoloogia osakond, Tartu Ülikool,
Ravila 14A, 50411 Tartu, Eesti
Kontakt: Tel. +372 58176460
E-post: kristjan.leben@ut.ee

Haridus

2016–... Tartu Ülikool, Geoloogia osakond, Geoloogia doktorant
2012–2015 Tartu Ülikool, MSc geotehnoloogias
2009–2012 Tartu Ülikool, BSc keskkonnatehnoloogias

Teenistuskäik

2021 – ... Tartu Ülikool, Geoloogia osakond, analüütik
2017 – 2020 Tartu Ülikool, Geoloogia osakond, geoloogia nooremteadur
2014 Tartu Ülikool, Geoloogia osakond, geoloogia spetsialist

Teadustöö põhisuunad:

Keskkonnageoloogia, geokeemia, mineraloogia

Publikatsioonid

1. **Leben, K.**; Mõtsep, R.; Paaver, P.; Konist A.; Pihu, T.; Paiste, P.; Heinmaa, I.; Nurk, G.; Anthony, E.; Kirsimäe, K. (2019). Long-term mineral transformation of Ca-rich oil shale ash waste. *Science of the Total Environment* 658, 1404–1415.
2. **Leben, K.**; Mõtsep, R.; Paaver, P.; Konist A.; Pihu, T.; Kirsimäe, K. (2020). Geochemical study of stable carbon and oxygen isotopes in landfilled Ca-rich oil shale ash. *Estonian Journal of Earth Sciences* 69 (3), 134–142.
3. **Leben, K.**; Mõtsep, R.; Konist A.; Pihu, T.; Kirsimäe, K. (2021). Carbon dioxide sequestration in power plant Ca-rich ash waste deposits. *Oil Shale* 38 (1), 65–88.

DISSERTATIONES GEOLOGICAE UNIVERSITATIS TARTUENSIS

1. **Пэп Мянник.** Конодонты в верхнеордовикских и нижнесилурийских отложениях Эстонии. Тарту, 1992, 355 с.
2. **Elvi Tavast.** Fennoskandia kilbi lõunanõlva ja sellega piirnevate alade aluspõhja reljeef. Tartu, 1992, 357 lk.
3. **Kaarel Orviku.** Characterisation and evolution of Estonian seashores. Tartu, 1992, 19 p.
4. **Анатолий Молодьков.** ЭПР-анализ скелетного вещества моллюсков в хроностратиграфических исследованиях позднего кайнозоя. Тарту, 1992, 33 с.
5. **Jaan Lutt.** Late- and postglacial deposits on the Estonian shelf. Tartu, 1993, 31 p.
6. **Reet Karukäpp.** Gotiglatsiaalne morfogenees Skandinaavia mandriliustiku kagusektoris. Tartu, 1997, 181 p.
7. **Argo Jõelet.** Geothermal studies of the Precambrian basement and Phanerozoic sedimentary cover in Estonia and Finland. Tartu, 1998, 125 p.
8. **Jüri Nemliher.** Mineralogy of Phanerozoic skeletal and sedimentary apatites: an XRD study. Tartu, 1999, 134 p.
9. **Kalle Kirsimäe.** Clay mineral diagenesis on the Lower Cambrian “Blue Clay” in the northern part of the Baltic Paleobasin. Tartu, 1999, 113 p.
10. **Jüri Plado.** Gravity and magnetic signatures of meteorite impact structures. Tartu, 2000, 87 p.
11. **Olev Vinn.** Morphogenesis and phylogenetic relationships of Clitambonitidines, Ordovician Brachiopods. Tartu, 2001, 127 p.
12. **Leho Ainsaar.** The middle Caradoc facies and faunal turnover in the late Ordovician Baltoscandian palaeobasin: sedimentological and carbon isotope aspects. Tartu, 2001, 109 p.
13. **Oive Tinn.** Early Ostracode evolution and Palaeoenvironmental application in the Ordovician of Baltoscandia. Tartu, 2002, 145 p.
14. **Maris Rattas.** Subglacial environments in the formation of drumlins — The case of the Saadjärve Drumlin Field, Estonia. Tartu, 2004, 117 p.
15. **Ene Kadastik.** Upper-Pleistocene stratigraphy and deglaciation history in northwestern Estonia. Tartu, 2004, 129 p.
16. **Helje Pärnaste.** Early Ordovician trilobites of suborder Cheirurina in Estonia and NW Russia: systematics, evolution and distribution. Tartu, 2004, 138 p.
17. **Mari-Ann Mõtus.** Silurian (Llandovery-Wenlock) tabulate corals of Baltoscandia: taxonomy, palaeoecology, distribution. Tartu, 2005, 167 p.
18. **Alar Rosentau.** Development of proglacial lakes in Estonia. Tartu, 2006, 114 p.
19. **Evelin Verš.** Development of impact-induced hydrothermal system at Kärkla impact structure. Tartu, 2006, 96 p.

20. **Sigitas Radzevičius.** The genus *Pristiograptus* in wienlock of East Baltic and the Holy Cross Mountains. Tartu, 2007, 133 p.
21. **Andres Marandi.** Natural chemical composition of groundwater as a basis for groundwater management in the Cambrian-Vendian aquifer system in Estonia. Tartu, 2007, 116 p.
22. **Eve Niinemets.** Vegetation and land-use history of the Haanja Heights (SE-Estonia) during the holocene. Tartu, 2008, 146 p.
23. **Kalle-Mart Suuroja.** Geology and lithology of the early palaeozoic marine impact structures Kärđla and Neugrund (Estonia). Tartu, 2008, 234 p.
24. **Rutt Hints.** Early diagenesis of Ordovician and Silurian Bentonites in the Northern Baltic Palaeobasin. Tartu, 2009, 90 p.
25. **Peeter Somelar.** Illitization of K-bentonites in the Baltic Basin. Tartu, 2009, 118 p.
26. **Ulla Preeden.** Remagnetizations in sedimentary rocks of Estonia and shear and fault zone rocks of southern Finland. Tartu, 2009, 121 p.
27. **Kati Tänavsuu-Milkeviciene.** Transgressive to regressive turnaround in the Middle Devonian Baltic Basin. Tartu, 2009, 106 p.
28. **Valle Raidla.** Chemical and isotope evolution of groundwater in the Cambrian-Vendian aquifer system in Estonia. Tartu, 2010, 134 p.
29. **Kadri Sohar.** Quaternary ostracods from Estonia and their application in palaeoenvironmental reconstruction. Tartu, 2010, 140 p.
30. **Kristjan Urtson.** Stepwise melt transport and accumulation: analogue and numerical modelling approach. Tartu, 2011, 83 p.
31. **Marko Kohv.** Landslides in clayey soils of western Estonia. Tartu, 2011, 116 p.
32. **Nele Muttik.** Post-impact alteration of impactites: Ries crater, Germany. Tartu, 2011, 78 p.
33. **Annette Sedman.** Strength and self-cementing properties of oil shale retorting wastes. Tartu, 2013, 82 p.
34. **Arkady Tsyrlunikov.** Complex seismo-acoustic and lithological study of the Lateglacial and postglacial sediments northern Gulf of Riga, eastern branch of the central Baltic Sea. Tartu, 2013, 102 p.
35. **Marge Uppin.** Geological sources and hydrochemistry of fluoride and boron in Silurian-Ordovician aquifer system. Tartu, 2013, 86 p.
36. **Peeter Talviste.** Temporal changes in weak natural and artificial soils – influence on geotechnical characteristics. Tartu, 2014, 204 p.
37. **Katrin Lasberg.** Chronology of the Weichselian Glaciation in the south-eastern sector of the Scandinavian Ice Sheet. Tartu, 2014, 100 p.
38. **Sirle Liivamägi.** Neoproterozoic Baltic paleosol: geology and palaeoenvironmental interpretation. Tartu, 2015, 94 p.
39. **Lauri Joosu.** Petrography and the rare earth element composition of apatite in 2 Ga Onega and Pechenga basins, Russia: the environmental settings for phosphogenesis. Tartu, 2015, 139 p.
40. **Liisa Lang.** Baculate shell structure in Early Palaeozoic linguliform brachiopods. Tartu, 2015, 114 p.

41. **Päärn Paiste.** Geopolymeric potential of the Estonian oil shale processing waste. Tartu, 2017, 125 p.
42. **Mikk Gaškov.** Stable isotope and fluid inclusion evidence of multistage fluidal activity in Baltic paleobasin: Silurian carbonate sequence in Kalana, Estonia. Tartu, 2017, 104 p.
43. **Viirika Mastik.** Silurian noncalcified macroscopic algal fossils from the Kalana *Lagerstätte*, Estonia. Tartu, 2018, 91 p.
44. **Kairi Põldsaar.** Soft-sediment deformation and gravity flow structures in the Lower Palaeozoic successions of the Baltic Basin. Tartu, 2019, 105 p.
45. **Timmu Kreitsmann.** Application of carbon isotope and rare earth elements as recorders of environmental conditions in the aftermath of the Paleoproterozoic Lomagundi-Jatuli Event. Tartu, 2020, 163 p.
46. **Triine Nirgi.** Holocene relative shore-level changes and geoarchaeology of the prehistoric sites in western Estonia. Tartu, 2020, 161 p.